Variability and controls on $\delta^{18}O$, d-excess, and $\Delta'^{17}O$ in southern Peruvian precipitation

P. G. Aron[1*], C. J. Poulsen[1], R. P. Fiorella[2], N. E. Levin[1], R. P. Acosta[1], B. J., Yanites[3], E. J. Cassel[4]

[1]Department of Earth and Environmental Sciences, University of Michigan, Ann Arbor, MI, USA, [2]Department of Geology and Geophysics, University of Utah, Salt Lake City, UT, USA, [3]Department of Earth and Atmospheric Sciences, University of Indiana, Bloomington, IN, USA, [4]Department of Geography and Geological Sciences, University of Idaho, ID, USA

Corresponding author: Phoebe Aron (paron@umich.edu)

Key Points:

- The isotopic composition of central Andean precipitation records upstream precipitation, local convection, and remote moisture sources
- Precipitation on the flank of the western central Andes is sourced from the Pacific Ocean
- $\Delta'^{17}O$ can separate evaporated and non-evaporated samples and provides key baseline information for Andean paleoclimate and paleoaltimetry

Abstract

The isotopic composition of precipitation is used to trace water cycling and climate change, but interpretations of the environmental information recorded in central Andean precipitation isotope ratios are hindered by a lack of multi-year records, poor spatial distribution of observations, and a predominant focus on Rayleigh distillation. To better understand isotopic variability in central Andean precipitation, we present a three-year record of semimonthly $\delta^{18}O_p$ and $\delta^{2}H_p$ values from 15 stations in southern Peru and triple oxygen isotope data, expressed as $\Delta'^{17}O_p$, from 32 precipitation samples. Consistent with previous work, we find that elevation correlates negatively with $\delta^{18}O_p$ and that seasonal $\delta^{18}O_p$ variations are related to upstream rainout and local convection. Spatial $\delta^{18}O_p$ variations and atmospheric back trajectories show that both eastern- and western-derived air masses bring precipitation to southern Peru. Seasonal d-excess$_p$ cycles record moisture recycling and relative humidity at remote moisture sources, and both d-excess$_p$ and $\Delta'^{17}O_p$ clearly differentiate evaporated and non-evaporated samples. These results begin to establish the natural range of unevaporated $\Delta'^{17}O_p$ values in the central Andes and set the foundation for future paleoclimate and paleoaltimetry studies in the region. This study highlights the hydrologic understanding that comes from a combination of $\delta^{18}O_p$, d-excess$_p$, and $\Delta'^{17}O_p$ data and helps identify the evaporation, recycling, and rainout processes that drive water cycling in the central Andes.

1 Introduction

The isotopic composition of precipitation ($\delta^{18}O_p$, $\delta^{17}O_p$, $\delta^{2}H_p$, where δ is defined as $(R_{sample}/R_{standard} - 1)*1000$, R is the ratio of heavy-to-light mass isotopes, and the subscript $_p$ refers to precipitation) and geologic materials that preserve precipitation isotope ratios are valuable tracers of water cycling and climate change. In the Andes mountains, $\delta^{18}O_p$ and $\delta^{2}H_p$ have been used to infer information about both modern and past water cycling (e.g., Fiorella et al., 2015a; Poulsen et al., 2010) as well as past climate conditions (e.g., Hardy et al., 2003). Nevertheless, uncertainties remain about the controls on modern $\delta^{18}O_p$, $\delta^{2}H_p$, and $\delta^{17}O_p$ in the Altiplano region (~ 12˚S to 22˚S and 63˚W to 74˚W, hereafter referred to as the central Andes) because there are relatively few observations of $\delta^{18}O_p$ and $\delta^{2}H_p$ and no observations of $\delta^{17}O_p$ (Figure 1a; Valdivielso et al., 2020). Moreover, most previous studies of central Andean precipitation isotope ratios focus primarily on either $\delta^{18}O_p$ or $\delta^{2}H_p$ and hydrologic processes (e.g., rainout) associated with equilibrium fractionation and Rayleigh distillation (e.g., Gonfiantini et al., 2001). These studies do not leverage the additional information that comes from a combination of $\delta^{18}O_p$ and $\delta^{2}H_p$ (d-excess$_p$; Dansgaard, 1964) and generally leave kinetic fractionation processes (e.g., evaporation at a moisture source or moisture recycling) unexplored. Additional observations of central Andean $\delta^{18}O_p$, $\delta^{2}H_p$, and $\delta^{17}O_p$ and an expanded emphasis on the isotopic signals of kinetic fractionation can improve understanding of water cycling, paleoclimate, and mountain uplift in the central Andes (e.g., Bird et al., 2011; Garzione et al., 2017).

The large-scale variability of central Andean $\delta^{18}O_p$ and $\delta^{2}H_p$ is primarily attributed to Rayleigh distillation during rainout (Dansgaard, 1964; Fiorella et al., 2015a; Gat, 1996; Gonfiantini et al., 2001; Jeffery et al., 2012; Rozanski et al., 1993; Sturm et al., 2007; Vimeux et al., 2005). However, Rayleigh distillation does not account for all of the observed variability, and central Andean $\delta^{18}O_p$ and $\delta^{2}H_p$ values can also reflect moisture recycling (Ampuero et al., 2020; Salati et al., 1979), the intensity of upstream and local convective precipitation (Fiorella et al.,

2015a; Guy et al., 2019; Samuels-Crow et al., 2014a; Valdivielso et al., 2020; Vimeux et al., 2005; Vimeux et al., 2011; Vuille et al., 2012; Vuille & Werner, 2005), and interactions between Atlantic and Pacific moisture sources (Aravena et al., 1999). Elsewhere, a combination of $\delta^{18}O_p$ and d-excess$_p$ has been used to identify evaporation at a moisture source (e.g., Pfahl & Sodemann, 2014), condensation from mixed-phase clouds (e.g., Bolot et al., 2013), and sub-cloud evaporation (e.g., Froehlich et al., 2008), but to date studies of d-excess$_p$ in the central Andes have received far less attention than those of $\delta^{18}O_p$ or $\delta^{2}H_p$. Additional efforts to understand d-excess variations in liquid water, water vapor, and ice cores can help explain the evaporation and condensation processes that are recorded in central Andean $\delta^{18}O$ and $\delta^{2}H$ data (e.g., Samuels-Crow et al., 2014b).

Triple oxygen isotope variations have recently emerged as another metric to track kinetic fractionation in waters (e.g., Li et al., 2017) and geologic materials (e.g., Passey et al., 2014). These variations, expressed as $\Delta'^{17}O$ (see Section 2.2 below), are useful because they add new information to $\delta^{18}O$ and/or $\delta^{2}H$ records by quantitatively separating equilibrium and kinetic fractionation (Barkan & Luz, 2007). Currently, however, measurements of triple oxygen isotope ratios are rare and there are only a few published observations of surface water $\Delta'^{17}O$ (Aron et al., 2021; Surma et al., 2018; Voigt et al., 2021) and structurally bonded gypsum water $\Delta'^{17}O$ (Herwartz et al., 2017) from the central Andes. Much like d-excess, water $\Delta'^{17}O$ measurements can help identify the controls on $\delta^{18}O$ and $\delta^{2}H$ and enable better understanding of hydrologic processes and climate conditions.

To better understand the environmental controls on precipitation isotope ratios in the central Andes, we report on a three-year dataset of $\delta^{18}O_p$, $\delta^{17}O_p$, and $\delta^{2}H_p$ data from a previously unstudied region in southern Peru (Figure 1b, Table S1). This dataset extends observations of $\delta^{18}O_p$ and $\delta^{2}H_p$ from Bolivia (Fiorella et al., 2015a; Gonfiantini et al., 2001) into southern Peru and fills a spatial gap across the northern Altiplano and western slope of the Peruvian Andes (Figure 1a). We show that a combination of $\delta^{18}O_p$, d-excess$_p$, and $\Delta'^{17}O_p$ can differentiate equilibrium and kinetic fractionation to constrain rainout, air mass sources, and moisture recycling and improve understanding of water cycling and climate change in the central Andes.

2 Background

2.1 Central Andes topography, precipitation, and atmospheric circulation

The central Andes in southern Peru, Bolivia, and northern Chile are split into the Eastern and Western Cordilleras, both of which reach over 6 km in height. The Altiplano lies between the Cordilleras and has lower elevation (~4 km) and lower relief. A strong hydrologic gradient extends across this region from the Amazon Rainforest, one of the wettest places on Earth, to the Atacama Desert, one of the driest (Figure 2). Moisture transport from the Amazon Basin and orographic uplift generate high precipitation rates (up to 6,000 mm/yr) on the flank of the Eastern Cordillera (Garreaud, 2009), while the Western Cordillera flank is exceptionally dry (< 20 mm/yr) due to upwelling of cold waters from the coastal Humboldt current, large-scale subsidence over the eastern Pacific Ocean, and orographic blocking from the Eastern Cordillera (e.g., Garreaud et al., 2002; Rodwell & Hoskins, 2001; Vuille et al., 2000).

Seasonally, the central Andes are wetter during the austral summer (December to March) and drier in the austral winter (June to September) (Figure 2). In the winter, upper-level (~200 hPa) circulation is dominated by subtropical westerly winds that restrict low-level (~850 hPa) easterly moisture from reaching the Altiplano (Figures 2b and 2d). In the summer, the westerly

winds weaken and shift southward, and stronger easterly winds transport moisture toward the central Andes. Simultaneously, intense summertime latent heating over the Amazon generates an upper-level (~200 hPa) high pressure circulation feature known as the Bolivian High (Lenters & Cook, 1997) that directs and intensifies near-surface moisture flow (Figure 2c). Orographic blocking forms the South American Low Level Jet (SALLJ, Figure 2a), a low-level (~850 hPa) barrier jet that transports moisture from the tropics to the subtropics and plays a critical role in South American hydrology (e.g., Insel et al., 2010; Vera et al., 2006).

Infrequent, small (generally < 10 mm/event) summer storms occur on the western central Andean slope when anomalously warm coastal sea surface temperatures break up the western flank inversion layer (Aceituno, 1988). Although this localized feature is most commonly associated with the negative phase of the El Niño Southern Oscillation (ENSO) and extreme precipitation events along the tropical coastal western Andes (e.g., Quinn & Neal, 1987; Takahashi & Martínez, 2019), it also generates episodic summertime precipitation on the western flank (e.g., Garreaud et al., 2002; Vuille et al., 2000). Wintertime precipitation is very rare on the western flank because sea surface temperatures are relatively cool and the inversion layer remains stable (Figures 2b and 2d; Rutllant et al., 2003).

2.2 Isotope systematics

Relationships between isotopic compositions (e.g., $\delta^{18}O$ vs. $\delta^{2}H$) are generally considered to be linear, but mass-dependent isotope fractionation actually follows a power law relationship that relates the fractionation factors (α) of coexisting phases (A and B) by a defined fractionation exponent (θ) (Matsuhisa et al., 1978; Young et al., 2002):

$$^{*}\alpha_{A\text{-}B} = (^{*}\alpha_{A\text{-}B})^{\theta} \quad (1)$$

where * denotes a heavy mass number (e.g., ^{17}O, ^{18}O, ^{2}H). The value of θ is derived from mass law theory (Criss, 1999; Matsuhisa et al., 1978; Young et al., 2002) and distinguishes equilibrium (θ_{eq}) and kinetic (θ_{diff}) processes. These θ values are more familiar as the slopes that relate isotopic compositions (α or δ values) during isotopic fractionation. Deviations in these slopes (or position relative to them) indicate different roles of equilibrium and kinetic fractionation on isotopic compositions.

The most familiar slope in isotope hydrology is the slope of the oxygen-hydrogen Global Meteoric Water Line (GMWL) (Craig, 1961). This empirical value (8) integrates equilibrium ($\theta_{eq} \approx 8$) and kinetic ($\sim 2.5 < \theta_{diff} < 8$; Gonfiantini et al., 2018) processes and establishes a reference frame from which d-excess is defined (Dansgaard, 1964):

$$\text{d-excess} = \delta^{2}H - 8*\delta^{18}O. \quad (2)$$

A similar reference relationship differentiates triple oxygen isotope ratios during equilibrium and kinetic fractionation and defines the $\Delta'^{17}O$ parameter (Barkan & Luz, 2007):

$$\Delta'^{17}O = \delta'^{17}O - 0.528*\delta'^{18}O. \quad (3)$$

The empirically determined slope of the triple oxygen isotope reference line (0.528) (Luz & Barkan, 2010; Meijer & Li, 1998) integrates equilibrium ($\theta_{eq} = 0.529$; Barkan & Luz, 2005) and

kinetic (θ_{diff} = 0.518; Barkan & Luz, 2007) fractionation. The $\Delta'^{17}O$ definition requires δ' notation ($\delta' = \ln(\delta/1000 + 1)*1000$; Hulston & Thode, 1965; Miller, 2002) because mass-dependent deviations from the triple oxygen isotope reference relationship are very small and must be calculated from a reference frame that is exactly linear.

3 Methods

3.1 Precipitation network and sample collection

This study includes data from a network of precipitation collection stations in southern Peru that extends from the western Peruvian Amazon (~13˚S) to near the Pacific coast (~17˚S) (Figures 1b and S1). Ten stations (San Gaban, Ollachea, Macusani, Ayaviri, Ichuña, Carumas, Majes, Ayo, Orcopampa, and Santo Tomas) were installed in May and June 2016; eight stations (Pampahuta, Ubinas, Quinistaquillas, Moquegua, Arequipa, Cotahuasi, and Puyca) were added in November 2017. The final station (Calca) was installed in July 2018. This study includes samples collected through May 2019 because travel restrictions associated with COVID-19 prevented travel after the 2020 rainy season. Isotopic data are not considered from Ichuña, Orcopampa, or Puyca due to compromised samples or from Ayo due to a lack of rain. Additional details about data quality and the stations are in Table S1 and Section 3.3.

Each precipitation collection station was managed by a local Peruvian observer and collocated alongside SENAMHI (Servicio Nacional de Meteorología e Hidrología del Perú) meteorological stations that record daily precipitation amount. Some SENAMHI stations also record mid-day relative humidity and maximum and minimum or morning and afternoon temperature. Temperature and relative humidity sensors (Onset HOBO, U23 Pro v2) were added to stations that only record precipitation. Mean annual temperature (MAT) and mean annual precipitation (MAP) from each site were extracted from the University of Delaware 0.5˚ monthly gridded climate data (1960-1990 average) (Legates & Willmott, 1990a, 1990b).

Precipitation samples were collected at each site on the 1st and 15th of every month. During the first year, samples were collected in 1.5 L HDPE bottles (McMaster Carr, 4280T37) following the description in Gröning et al. (2012). This oil-free collection technique prevented evaporation and simplified sample collection because station observers did not have to separate the sample water from overlaying oil. Station observers poured the collected precipitation into 20 ml HDPE storage vials (Wheaton, 986716), capped the storage vials with PolyCone caps, and cleaned and dried the collection bottle. After the first year, observers added mineral oil to the collection bottles as another measure to prevent evaporation because we determined that the traditional mineral oil technique is more reliable in remote locations and with non-expert observers (Friedman et al., 1992; Scholl et al., 1996). Observers used a syringe to extract sample water and cleaned, dried, and added a new layer of oil to the collection bottles between samples.

During annual site visits, we gathered the precipitation samples, cleaned and repaired the collection equipment, and interviewed observers about local weather conditions. In the lab, we transferred samples into 16 ml glass vials with PolyCone caps (The Lab Depot, 316018-2170) for secure long-term storage. At most, samples were stored in HDPE vials for one year, so they are not compromised by fractionation with the plastic containers (Spangenberg, 2012).

3.2 Isotopic analysis

The $\delta^{18}O$ and $\delta^{2}H$ values of every precipitation sample were measured using a Picarro L2130-i with a high-precision vaporizer (A0211) and attached autosampler. Picarro

ChemCorrect software screened samples for organic contamination and normalized raw $\delta^{18}O$ and $\delta^{2}H$ values to the VSMOW-SLAP scale with four in-house liquid standards that were calibrated with USGS reference waters (USGS45, 46, 49, and 50). Analytical precision of repeat analyses of deionized water was better than 0.1‰ and 0.3‰ for $\delta^{18}O$ and $\delta^{2}H$, respectively. Assuming the errors on $\delta^{18}O$ and $\delta^{2}H$ are independent, the analytical precision of d-excess is better than 0.4‰.

The $\delta^{18}O$ and $\delta^{17}O$ values of 32 precipitation samples were measured with a dual-inlet Nu Perspective isotope ratio mass spectrometer (IRMS) using the cobalt(III) fluoride method developed by Baker et al. (2002) and refined by Luz and Barkan (2005). Our methods are described in Aron et al. (2021). Triple oxygen isotope values were normalized to the VSMOW-SLAP scale using values of 0.0000‰ for $\delta^{18}O_{VSMOW}$ and $\delta^{17}O_{VSMOW}$ (Gonfiantini, 1978), –55.5000‰ for $\delta^{18}O_{SLAP}$, and –29.6986‰ for $\delta^{17}O_{SLAP}$ (Schoenemann et al., 2013). The root-mean-square error of the IRMS measurements, determined from replicate analyses of USGS reference waters (Table S2), was 0.2‰ for $\delta^{17}O$, 0.3‰ for $\delta^{18}O$, and 6 per meg for $\Delta'^{17}O$. The analytical precision of $\Delta'^{17}O$ is better than that of $\delta^{17}O$ and $\delta^{18}O$ because any fractionation that occurs during sample preparation is related by a $\delta'^{18}O$–$\delta'^{17}O$ slope that is nearly equivalent to the value of the reference slope (Barkan & Luz, 2007; Landais et al., 2006; Schoenemann et al., 2013).

3.3 Isotopic data caveats

We collected and analyzed $\delta^{18}O$ and $\delta^{2}H$ from a total of 451 precipitation samples (Table S1). From this, we removed 12 samples with negative d-excess$_p$ values that are likely affected by evaporation and 130 samples from five sites that we suspect were collected from tap or surface water sources. The probable tap or surface water samples were easily identifiable from site-specific timeseries with less than 1‰ of seasonal $\delta^{18}O_p$ variation (seasonal $\delta^{18}O_p$ variation is at least 5‰ at most sites). All the measured $\delta^{18}O$ and $\delta^{2}H$ data are reported in Table S3, but data from the excluded samples are flagged as unreliable.

Data are also missing or incomplete from three other sites. First, data from Macusani are missing from May 2018 to May 2019 because the observer did not record collection dates on the sample vials. Second, sample collection lasted only one year (June 2017 to May 2018) in Cusco. Third, the observer in Majes was not available during the 2019 site visit, so isotopic data from this site only extend until May 2018.

After screening for compromised and/or improperly collected samples, the final dataset contains 309 precipitation samples (Table S1).

3.4 Air mass trajectories

We used the Hybrid coordinate Single Parcel Lagrangian Integrated Trajectory model (HYSPLIT; Draxler & Hess, 1998) and 0.5˚ Global Data Assimilation System (GDAS) meteorological data to compare eastern and western moisture sources at San Gaban, Ayaviri, Santo Tomas, Cotahuasi, Ubinas, Majes, and Moquegua. At each site, ten-day atmospheric back trajectories were initiated at 0, 6, 12, and 18 UTC (the availability of GDAS data) from 1,000 m above ground level. We chose the initiation height based on previous back trajectory analyses in the central Andes (e.g., Fiorella, et al., 2015a; Vimeux et al., 2011). Parcel vertical velocities were determined from GDAS wind fields. To separate winds on wet and dry days, we analyzed the trajectories in two ways: an ‘all days’ analysis that included trajectories from every day

during the study period and a 'rainy days' analysis that only included the trajectories initiated on days when rain fell at each site.

We then used the Lagrangian tracer developed by Sodemann et al. (2008) to determine the humidity contribution from each grid cell along the moisture trajectories and calculate moisture footprints for each site (Figure S2). This iterative tracer links precipitation to remote evaporation sources by tracking increases in planetary boundary layer specific humidity and diagnoses the humidity contribution from each point along a trajectory. HYSPLIT-extracted boundary layer heights were doubled, as prior work with this tracer has suggested that using unscaled boundary layer heights may underestimate moisture contributions from shallow convection (Aemisegger et al., 2014; Fiorella et al., 2018; Sodemann et al., 2008). The ten-day trajectories used in this study were sufficiently long to determine moisture source locations for 85-95% of the total parcel moisture.

Finally, we determined the large-scale contribution of eastern and western air masses to precipitation in southern Peru by estimating the humidity contributions from two zones separated by the spine of the Western Cordillera: an eastern zone that includes humidity sourced from the Atlantic Ocean, Amazon Basin, eastern Andean flank, and the Altiplano and a western zone that includes humidity from the Pacific Ocean and western Andean flank. The ratio of eastern and western air masses was determined at each site by summing the monthly humidity contributions from each zone and dividing by the total moisture footprint across both zones. Because rain did not fall equally across the study region, we report the moisture flux ratios as quarterly seasonal averages among water years (a water year is defined as June to May to keep the summer rainy season intact). This approach is not intended to differentiate tropical versus extratropical air masses and is not well suited to identify small-scale circulation features along the Andean flanks or Altiplano due to the spatial and temporal scale of the GDAS data.

4 Results

4.1 Precipitation $\delta^{18}O$, $\delta^{2}H$, and d-excess

Values of $\delta^{18}O_p$ in southern Peru range from –29.3 to 2.0‰, $\delta^{2}H_p$ ranges from –216.1 to 35.2‰, and d-excess ranges from 0.2 to 41.8‰ (Figure 3a, Table S3). $\delta^{18}O_p$ and $\delta^{2}H_p$ are strongly correlated (Pearson's $r > 0.99$) and cluster on or near the $\delta^{18}O$-$\delta^{2}H$ GMWL, although the slope (8.1) and intercept (15.8) through $\delta^{18}O_p$ and $\delta^{2}H_p$ are slightly higher than the reference values (8 and 10, respectively). Because $\delta^{18}O_p$ and $\delta^{2}H_p$ are so strongly correlated, the following results and discussion focus only on $\delta^{18}O_p$ and d-excess$_p$.

Values of $\delta^{18}O_p$ and d-excess$_p$ varied on semimonthly to interannual timescales across the study region (Figure 4). The most pronounced temporal variation was a seasonal pattern on the eastern flank and Altiplano with lower rainy season (DJFM) $\delta^{18}O_p$ (–26.0 to –3.3‰, amount-weighted average –14.9‰) and d-excess$_p$ (2.4 to 33.6‰, amount-weighted average 14.6‰) values and higher dry season (JJAS) $\delta^{18}O_p$ (–21.1 to 2.0‰, amount-weighted average –7.5‰) and d-excess$_p$ (8.6 to 38.8‰, amount-weighted average 16.0‰) values. Seasonal $\delta^{18}O_p$ and d-excess$_p$ variability cannot be assessed on the western flank because precipitation only fell during the wet season, but in general western flank $\delta^{18}O_p$ (–16.7 to 1.2‰, amount-weighted average –6.7‰) values were higher and d-excess$_p$ (0.2 to 27.0‰, amount-weighted average 11.3‰) values were lower than those on the Altiplano or eastern flank (Figures 4 and 5).

Spatially, wet season amount-weighted $\delta^{18}O_p$ correlated negatively with elevation ($r = –0.82$, $p < 0.001$, Figures 5b and 6a) and latitude ($r = –0.72$, $p < 0.005$, Figure 6c) and exhibited weaker correlations with MAP ($r = –0.22$, $p = 0.67$, Figure 6b) and longitude ($r = –0.12$, $p = 0.46$). We report and show (Figures 5 and 6) amount-weighted averages from the wet season because dry season precipitation data do not exist on the western flank and most of the Altiplano. However, the relationships between amount-weighted annual $\delta^{18}O_p$ and elevation ($r = –0.84$), latitude ($r = –0.70$), longitude ($r = –0.13$), and MAP ($r = –0.20$) are nearly identical to those that only consider wet season data because most precipitation fell during the wet season. Stepwise multiple linear regression models with elevation, latitude, longitude, and MAP as possible predictor variables (Bowen & Wilkinson, 2002; Lechler & Niemi, 2011) confirm that elevation and latitude were the dominant controls on $\delta^{18}O_p$ (Table S4). Each regression model was assessed with the Akaike information criterion (AIC), with lower AIC scores indicating a balance between goodness of model fit with model parsimony.

Isotopic lapse rates were determined by linear regression through amount-weighted rainy season $\delta^{18}O_p$ from San Gaban, Ollachea, and Macusani on the eastern flank and Moquegua, Quinistaquillas, Carumas, Ubinas, Arequipa, Majes, and Cotahuasi on the western flank. The eastern flank $\delta^{18}O_p$ lapse rate, –2.8 ± 0.2‰/km, was determined from precipitation collected at three closely-located sites that span over 3.6 km of elevation, but this lapse rate does not change if $\delta^{18}O_p$ data from Cuzco, Calca, Ayaviri and/or Santo Tomas are also included in the regression analysis. The western flank $\delta^{18}O_p$ lapse rate was determined from all the available rainy season western slope precipitation data because rain events in this region are very rare. This $\delta^{18}O_p$ lapse rate is nearly identical when derived from all the western flank sites (–4.5 ± 1.2‰/km) and from the four sites (Moquegua, Quinistaquillas, Carumas, and Ubinas) in the Moquegua region (–4.3 ± 1.8‰/km). However, due to the small number of samples, interannual variability of western flank $\delta^{18}O_p$ lapse rates was high, ranging from –1.9‰/km in 2017 to –5.5‰/km in 2019, and the

uncertainty of the lapse rate (1.2‰/km) is an order of magnitude greater than that on the eastern flank (0.2‰/km).

Amount-weighted wet season d-excess$_p$ values ranged from 5.0 to 22.1‰ and are poorly correlated with elevation (r = 0.34, p = 0.24, Figures 5c and 6d), latitude (r = 0.16, p = 0.60, Figure 6f), or MAP (r = 0.07, p = 0.82, Figure 6e). Unfortunately, the observer at Carumas did not collect samples properly after 2017, so it is difficult to assess the noticeably high (22.1‰) d-excess$_p$ value at this site. Excluding this value, amount-weighted DJFM d-excess$_p$ was highest at Macusani (17.3‰) and decreased across the Altiplano from the Eastern Cordillera towards the Western Cordillera, with lower values on the western flank (5.0 to 13.3‰) than on the Altiplano or eastern flank (12.4 to 17.3‰) (Figure 5c).

4.2 Triple oxygen isotope ratios

Precipitation samples from San Gaban (n = 9), Ollachea (n = 2), Macusani (n = 6), Santo Tomas (n = 3), Ayaviri (n = 6), Carumas (n = 2), and Majes (n = 4) were selected for triple oxygen analysis to explore $\Delta'^{17}O_p$ relationships with d-excess$_p$, $\delta^{18}O_p$, elevation, MAP, and latitude (Figures 6 and 7). Among this subset of samples, $\delta'^{18}O_p$ ranges from –28.3 to –0.2‰, $\delta'^{17}O_p$ ranges from –14.9 to –0.1‰, and $\Delta'^{17}O_p$ ranges from 1 to 55 per meg (Figures 3b and 7a, Table S2). Although $\delta'^{18}O_p$ and $\delta'^{17}O_p$ are very well correlated (r > 0.99999) and appear to plot exactly on the reference relationship (Figure 3b), the slope (0.5275 ± 0.0003) of the observed $\delta'^{18}O_p$-$\delta'^{17}O_p$ regression line is slightly lower than that of the reference line (0.528). These small, mass-dependent $\delta'^{18}O$ and $\delta'^{17}O$ deviations from the reference line are not visible in Figure 3b, but become apparent when triple oxygen isotope data are shown as $\delta'^{18}O$ versus $\Delta'^{17}O$ (Figure 7a). This isotope space is analogous to plots of $\delta^{18}O$ versus d-excess (Figure 7b) and is an easier way to visualize isotopic compositions that vary on different orders of magnitude (1‰ is equal to 1,000 per meg).

Similar to most previously published water triple oxygen isotope data, $\Delta'^{17}O_p$ is slightly anticorrelated with $\delta'^{18}O_p$ (r = –0.26, Figure 7a) and positively correlated with d-excess$_p$ (r = 0.46, Figure 7c). In general, $\Delta'^{17}O_p$ was higher on the Altiplano (29 to 55 per meg) and lower on the dry western flank (1 to 35 per meg). Site-specific $\Delta'^{17}O$ variation was larger on the western flank (17 per meg $\Delta'^{17}O_p$ range at Carumas, 27 per meg at Majes) than on the eastern flank (12 per meg at San Gaban, 2 per meg at Ollachea). Across the study region, $\Delta'^{17}O_p$ was moderately positively correlated with elevation (r = 0.57, Figure 6g) and latitude (r = 0.41, Figure 6i) and uncorrelated with MAP (r = –0.07, Figure 6h). This dataset is not well suited to evaluate temporal $\Delta'^{17}O_p$ variability (Figure S3) and seasonal $\Delta'^{17}O_p$ variability should be the focus of future work.

4.3 Atmospheric moisture transport

The ratio of eastern- versus western-sourced air masses differs in the ‘all days’ (Figure 8, yellow squares) and the ‘rainy days’ (Figure 8, blue circles) analyses, but both reveal a dominant easterly source of water vapor on the eastern flank and a mixture of eastern and western sourced air masses on the central Altiplano and western flank (Figures 8 and S2). Across the study region, the ‘all days’ eastern moisture flux ratio decreased from > 99% on the eastern flank (Figure 8a), to ~ 75% on the central Altiplano (Figures 8b and 8c), ~ 30% high on the western flank (Figures 8d and 8e), and < ~ 10% at low elevation on the western flank (Figures 8f and 8g). The moisture flux ratio is more variable when calculated from the ‘rainy days’ trajectories, but

still shows that > 95% of the water vapor in San Gaban originated from the Atlantic Ocean and Amazon Basin (Figure 8a). The eastern-sourced 'rainy days' moisture flux ratio was also dominant at the high elevation sites during the 2018 and 2019 water years. During the 2017 water year, the contribution of western-sourced air masses to the high elevation sites was higher, ranging from ~40% to more than 70% (Figures 8b-8e).

Finally, it is interesting to compare the 'all days' and 'rainy days' moisture flux ratios on the western flank. For example, the 'all days' ratios show a dominant contribution from western-sourced air masses at high (Cotahuasi and Ubinas, ~ 75% of air masses) and low (Majes and Moquegua, > 90% of air masses) elevation. Such a clear distinction between air mass source regions disappears among the western flank 'rainy days' moisture flux ratios (Figures 8b-8e). This suggests that dry winds on the western flank of the central Andes originate predominantly from the Pacific Ocean, whereas the air masses that bring precipitation to this region are sourced from a combination of both eastern and western regions.

5 Discussion

5.1 Controls on central Andean $\delta^{18}O_p$

The seasonal $\delta^{18}O_p$ pattern observed on the eastern flank and Altiplano in southern Peru is consistent with previous studies from the central Andes (Figure 9a; Aravena et al., 1999; Fiorella et al., 2015a; Fritz et al., 1981; Gonfiantini et al., 2001; Guy et al., 2019) and is related to a number of hydrologic processes that contribute to lower $\delta^{18}O_p$ values during the summer rainy season. First, during the wet season, high upstream precipitation in the Amazon Basin decreases the isotopic composition of vapor that is advected to the central Andes (Fiorella, et al., 2015a; Guy et al., 2019; Vimeux et al., 2005, 2011). Second, rainy season deep convection and downdrafts from aloft entrain isotopically light vapor from the upper and middle troposphere and decrease $\delta^{18}O_p$ values (Blossey et al., 2010; Galewsky et al., 2016; Moore et al., 2014; Risi et al., 2008; Samuels-Crow et al., 2014a; Worden et al., 2007). Although small, localized convective cells can entrain near-surface vapor with relatively high isotopic compositions (e.g., Aggarwal et al., 2016; Kurita, 2013), the high elevation Altiplano and intense daytime heating across the Amazon Basin lead to the development of deep convective cells (Garreaud et al., 2009) that decrease $\delta^{18}O_p$ values in this region. Third, water droplets likely undergo less sub-cloud evaporation and less heavy isotope enrichment during the wet season when relative humidity is high and the air column is closer to saturation than during the dry season.

The interannual variations of central Andean $\delta^{18}O_p$ are often linked to ENSO (e.g., Vuille & Werner, 2005), but our study duration is short and occurred during weak ENSO conditions (National Weather Service, Climate Prediction Center) and we do not observe consistent interannual $\delta^{18}O_p$ patterns (Figures 4a, 4b, and 5b). Interestingly, the relatively strong contribution of western-sourced water vapor during the 2017 water year (Figures 8b-8g and Figure S2), which is likely related to the strong El Niño event that occurred off the coast of Peru and Ecuador in early 2017 (Garreaud et al., 2018; Peng et al., 2019), is not evident in the western flank or Altiplano $\delta^{18}O_p$ data (Figures 4 and 5). Although this precipitation record is too short to comment substantially on interannual $\delta^{18}O_p$ variability, the absence of a clear ENSO-$\delta^{18}O_p$ relationship shows that even strong El Niño events are not always reflected in local precipitation isotope ratios. Instead, it is possible that rainout over the Andes overwrites $\delta^{18}O_p$ anomalies related to Pacific Ocean conditions and/or regional atmospheric circulation (Hurley et al., 2019; Thompson et al., 2017).

Site-to-site correlations of concurrent semimonthly $\delta^{18}O_p$ values (Table S5) reflect a combination of synoptic- and local-scale controls on $\delta^{18}O_p$ in southern Peru. Strong correlations between eastern flank and eastern Altiplano $\delta^{18}O_p$ values indicate synoptic-scale moisture transport, whereas weaker correlations among western flank sites result from sporadic and small-scale precipitation events (Figure 4). Large (up to 15‰) variations between concurrent semimonthly $\delta^{18}O_p$ values on the Altiplano point to local-scale $\delta^{18}O_p$ controls such as convection and near-surface convergence (Garreaud et al., 2003; Kumar et al., 2019; Romatschke & Houze, 2010), ridges and valleys that funnel moisture (Giovannettone & Barros, 2009), or the addition of water vapor from evaporation of lakes or other surface water (Pillco Zolá et al., 2019).

Our analysis of regional $\delta^{18}O_p$ controls shows that 1) elevation is a dominant control on $\delta^{18}O_p$ values (Figure 6a, Table S4) and 2) central Andean $\delta^{18}O_p$ values are not correlated with local precipitation amounts on annual ($r = –0.06$, our data), rainy season ($r = –0.05$, all monthly data), monthly ($r = –0.08$, all monthly data), or semimonthly ($r = 0.13$, our data) time scales (Figure 6b). Although our dataset only contains data from three years, these results are consistent with previous work from the central Andes and suggests that local precipitation rates are often poor predictors of precipitation isotope ratios in the central Andes (e.g., Vimeux et al., 2005). There is a clear seasonal signal in $\delta^{18}O_p$ with lower values during the rainy season and higher values during the dry season (Figures 4a and 9a), but individual $\delta^{18}O_p$ values are more closely tied to upstream rainout, evapotranspiration, moisture convergence, and cloud type than local precipitation amount in the central Andes (Konecky et al., 2019). The statistically significant latitude-$\delta^{18}O_p$ relationship (Table S4) in southern Peru is unique in the central Andes (Figure 6c) and is opposite in sign from the global trend because the global latitude-$\delta^{18}O_p$ relationship is related to progressive rainout during poleward moisture transport (Bowen et al., 2019) whereas the latitude-$\delta^{18}O_p$ relationship in southern Peru reflects a contribution of eastern- and western-derived water vapor (Figure 8).

5.2 Hydrologic interpretations of d-excess and $\Delta'^{17}O$

To this point, interpretations of isotopic variability have mainly focused on large-scale circulation patterns, rainout, and convection. However, processes such as evaporation, moisture recycling, and in-cloud microphysics also affect the isotopic composition of precipitation but are poorly constrained with $\delta^{18}O_p$ alone. Here, we show how d-excess and $\Delta'^{17}O$ complement $\delta^{18}O$ to provide new hydrologic insights in the central Andes.

We observe high (>10‰) d-excess$_p$ values and two primary types of d-excess$_p$ variation: 1) a consistent 5-10‰ seasonal cycle with higher (> ~ 15‰) d-excess$_p$ values in the dry season and lower (~ 10-15‰) d-excess$_p$ values in the wet season and 2) infrequent very high (>25‰) dry season d-excess$_p$ values on the Altiplano (Figures 4c, 4d, and 9b). Regardless of season or location, d-excess is unrelated to elevation, MAP, or latitude (Figures 6d-6e) because it is primarily sensitive to kinetic fractionation.

The seasonal d-excess$_p$ pattern records relative humidity above the surfaces of remote Atlantic moisture sources and in the atmosphere above precipitation stations as well as land-atmosphere water fluxes from the Amazon (Salati et al., 1979). During the rainy season, d-excess$_p$ values from ~ 10 to 15‰ are consistent with Rayleigh distillation and moisture recycling across the Amazon Basin (Ampuero et al., 2020; Salati et al., 1979). During the dry season, lower relative humidity above the tropical Atlantic increases kinetic fractionation during evaporation and results in higher vapor d-excess (Pfahl & Sodemann, 2014). Downstream

condensation retains this signal, resulting in higher (> ~ 15‰) dry season d-excess$_p$ values (Figures 5c and 9b). Subcloud evaporation, which is more likely in the winter when the atmosphere is drier, may also play a role in the higher winter d-excess$_p$ values if precipitation condenses from reevaporated vapor (e.g., Risi et al., 2008). Evapotranspiration from the Amazon Basin may amplify this d-excess$_p$ seasonality if the bare-ground evaporation flux increases during the dry season (Pattnayak et al., 2019).

The very high (>25‰) Altiplano d-excess$_p$ values are uncommon in tropical precipitation, but are occasionally observed in the central Andes (Fiorella et al., 2015a; Guy et al., 2019; Vimeux et al., 2011) and other high elevation regions (Liotta et al., 2006). Guy et al. (2019) also observed high (>30‰) event-scale d-excess$_p$ values on the eastern margin of the Altiplano in 2016 and 2017. Such elevated d-excess$_p$ values likely reflect kinetic fractionation during ice crystal formation and deep convection over the central Andes (Bolot et al., 2013; Jouzel & Merlivat, 1984), low temperature condensation from upper troposphere water vapor (Bony et al., 2008; Galewsky et al., 2016; Samuels-Crow et al., 2014b), and/or a non-linear isotope effect in air parcels that have experienced strong rainout (Dütsch et al., 2017; Jouzel & Merlivat, 1984).

This study reports the first $\Delta'^{17}O_p$ data from the central Andes. Controls on $\Delta'^{17}O_p$ variation are not yet well established, so as a starting point we base explanations of $\Delta'^{17}O_p$ variation on our understanding of d-excess$_p$. In the same way d-excess records information about kinetic fractionation, we expect that $\Delta'^{17}O$ records information about evaporation, relative humidity near precipitation collection sites and above remote moisture sources, evapotranspiration and moisture recycling across the Amazon Basin, ice crystal formation, and/or condensation that incorporates upper troposphere water vapor. We also consider the role of air mass mixing, which produces a non-linear response in $\Delta'^{17}O$ because $\Delta'^{17}O$ is defined from logarithmic δ' values (Equation 2). A similar signal of mixing is likely less clear in d-excess because d-excess is defined from δ values (Equation 1) and the mixing response is linear.

The clearest findings from the triple oxygen isotope data are that 1) the range of $\Delta'^{17}O_p$ values (~ 20 to 40 per meg) in southern Peru is consistent with previous observations from other tropical and mid-latitude regions and 2) precipitation $\Delta'^{17}O$ values are less variable than those from surface water (Figure 7). A similar, more familiar distinction between precipitation and surface water is also observed in d-excess (Figures 7b and 7c) because surface waters are typically more evaporated than precipitation.

Interpretations of the variations among $\Delta'^{17}O_p$ observations are less clear. Most $\Delta'^{17}O_p$ values cluster around 20 to 40 per meg due to kinetic fractionation that occurs as water vapor diffuses through unsaturated air during the initial evaporation from moisture sources (Aron et al., 2021; Luz & Barkan, 2010). The same process results in d-excess$_p$ values from ~10 to 20‰ for these samples. These $\Delta'^{17}O_p$ and d-excess$_p$ values are higher than those of seawater (0 per meg and 0‰, respectively) because kinetic fractionation slopes are shallower than the slopes of the $\delta'^{18}O$–$\delta'^{17}O$ and $\delta^{18}O$–$\delta^{2}H$ reference relationships and evaporated vapor $\delta^{18}O$, $\delta^{17}O$, and $\delta^{2}H$ values fall above the reference lines. Positive $\Delta'^{17}O$ and d-excess values are then conserved through downstream condensation (Aron et al., 2021; Luz & Barkan, 2010). However, while the 10‰ d-excess$_p$ range in Figures 5 and 9 is interpretable, patterns among the $\Delta'^{17}O_p$ data from 20 to 40 per meg are not clearly related to seasonality, location, or moisture recycling and it is hard to definitively isolate competing fractionating processes within this 20 per meg range. For example, it is tempting to attribute some of the higher (~30 to 40 per meg) values at San Gaban to moisture recycling from the Amazon Basin or link regional $\Delta'^{17}O_p$ variability to eastern and

western moisture sources, but these interpretations are not yet clear from the $\Delta'^{17}O_p$ data and require further study.

Beyond the clustered $\Delta'^{17}O_p$ data from 20 to 40 per meg, we observe a few high (> 40 per meg) $\Delta'^{17}O_p$ values from sites located on the eastern margin of the Altiplano and two samples from Majes with relatively low (< 10 per meg) $\Delta'^{17}O_p$ values (Figures 7a and S3). The samples with high $\Delta'^{17}O_p$ values also have high (> 25‰) d-excess$_p$ values (Figure 7c), so it is likely that these $\Delta'^{17}O_p$ values are related to kinetic fractionation during ice crystal formation and/or condensation that incorporates upper troposphere water vapor. Future work to evaluate $\delta'^{17}O$ and $\delta'^{18}O$ during ice crystal formation and additional observations of $\Delta'^{17}O_p$ variability through the troposphere can test these interpretations (Risi et al., 2013). It is unlikely that the high $\Delta'^{17}O_p$ values are related to air parcels that have experienced strong rainout because $\Delta'^{17}O$ and d-excess typically diverge at low $\delta^{18}O$ values (Aron et al., 2021). The low $\Delta'^{17}O_p$ values at Majes are not related to evaporation (d-excess$_p$ of these samples is ~ 15‰) and instead could be indicative of air mass mixing on the western flank (Figure 8f).

Initial central Andean $\Delta'^{17}O_p$ results show the promise of this type of measurement in isotope-based studies of hydrology and climate. Primarily, these data clearly show that $\Delta'^{17}O$ can separate evaporated samples from non-evaporated samples (Figure 7). This sensitivity has exciting applications in paleoclimate studies, which have long been limited by a singular focus on either $\delta^{18}O$ (e.g., pedogenic carbonates) or $\delta^{2}H$ (e.g., leaf waxes or volcanic glass). The central Andes are a prime region of interest for future triple oxygen isotope studies because the history of Andean uplift is uncertain and many of the archives that are used to infer paleoaltimetry are from arid regions subject to a high degree of evaporation (Fiorella et al., 2015b). In this context, $\Delta'^{17}O$ will be a useful metric to differentiate isotopic signals that record information about paleoclimate conditions from those that reflect uplift or mountain building (Rech et al., 2019). Specifically, $\Delta'^{17}O$ can help diagnose evaporation on the Altiplano and Atacama Desert and may also contain new information about large-scale changes in moisture recycling and atmospheric circulation associated with the evolution of the Amazon Rainforest and uplift of the Andes mountains. Alongside these geologic applications, future hydrologic $\Delta'^{17}O$ studies should further evaluate the range of unevaporated $\Delta'^{17}O_p$, temporal $\Delta'^{17}O_p$ variation, and the relationship between $\Delta'^{17}O_p$ and elevation. These future studies are important because the positive correlation between $\Delta'^{17}O_p$ and elevation is almost certainly biased by the very high $\Delta'^{17}O_p$ values on the Altiplano (Figure 6g) and will likely weaken with future observations (Bershaw et al., 2020). Similarly, the trend between latitude and $\Delta'^{17}O$ (Figure 6i) is largely related to water types because lakes tend to have lower $\Delta'^{17}O$ values than precipitation and will also likely weaken with additional observations from this region.

5.3 Implications of western-derived air masses

Atmospheric back trajectories and isotopic data show an important role of western-sourced water vapor in southern Peru. A similar moisture source has been inferred from $\delta^{18}O_p$ in northern Chile and the Atacama Desert (Aravena et al., 1999; Herrera et al., 2018; Valdivielso et al., 2020), but is generally disregarded in modern central Andean water budgets (e.g., Garreaud, 1999) and is not considered in most reconstructions of Andean paleoaltimetry (e.g., Garzione et al., 2006). Our $\delta^{18}O_p$, d-excess$_p$, and moisture flux results show that western-sourced moisture may play an important hydrologic role in the dry western central Andes and may contribute to steep $\delta^{18}O_p$ lapse rates (–4.4 ± 1.1‰/km in southern Peru (this study) to ~–10‰/km in northern

Chile (Aravena et al., 1999; Fritz et al., 1981)) on the western flank where low elevation Pacific sourced water vapor (high $\delta^{18}O$) mixes with high elevation Atlantic sourced water vapor (low $\delta^{18}O$). Our results suggest that this moisture source should be considered in regional hydrologic assessments and paleoaltimetry reconstructions.

6 Conclusion

We report on a new three-year record of semimonthly $\delta^{18}O_p$, d-excess$_p$, and $\Delta'^{17}O_p$ from southern Peru to improve our understanding of water cycling and isotopic variation in the central Andes. We observe a strong negative $\delta^{18}O_p$ relationship with elevation and a seasonal $\delta^{18}O_p$ cycle related to upstream precipitation and local deep convection. These findings are consistent with previous work and are generally explained by equilibrium isotope fractionation. Kinetic fractionation is much less commonly considered in interpretations of central Andean precipitation isotope ratios, but can be quantified with d-excess and $\Delta'^{17}O$. Seasonal variations of d-excess$_p$ reflect moisture recycling, relative humidity above precipitation collection stations and at remote moisture sources, and regional evapotranspiration. This study reports the first $\Delta'^{17}O_p$ data from the central Andes and results clearly show that $\Delta'^{17}O$ differentiates evaporated and non-evaporated samples. This sensitivity has immense potential to quantify evaporation in paleoclimate studies and address outstanding questions about uplift and long-term climate change in the Andes. Although the modern hydrologic applications of $\Delta'^{17}O_p$ will require future work, our results show that d-excess$_p$ and $\Delta'^{17}O_p$ complements $\delta^{18}O_p$ data and record new information about water cycling. Together, these results highlight the utility and untapped potential of precipitation isotope ratios to understand water cycling, hydrologic conditions, and climate change in the central Andes.

Acknowledgments, Samples, and Data

We thank the many individuals in Peru who supported this project and collected precipitation samples. This includes: Edgar Garcia Peña, Jose Antonio Luna Zapata, Sixto Flores Sancho, Jose Dionicio Cardenas Roque, Franco Rufino Bedoya Prado, Elsa Elizabeth Monesimos Aliaga, Lenor Abila de Morocc, Rosalio Washington Coaquira, Monica Quispe Ramos, Fanny Cahouana, Julia Socorro Villca, Yisenia Lopez Vilco, Fernando Apaza Vilca, Sonia Pari Zapana, Alberto Arana Mamani, Juana Lidra Apaza Cari, Francisco Ligue, Susana Gonzalez Yañez, Erick Diego Ramos Gonzalez, Rolando Palamo Ticona, Pascual Merma Ortiz, Julio Manzano Sanchez, Rosa, Lucio, Pascula, and Roque Zanabria Alvarado. This work was supported by NSF Tectonics Program award 1550101. In addition, PGA received support from a Rackham Predoctoral Fellowship, two Rackham Graduate Student Research Awards, a Rackham International Research Award, and the Scott Turner Award from the Department of Earth and Environmental Sciences at the University of Michigan. RPF acknowledges support from NSF award 1954660. Triple oxygen isotope analyses were supported by start-up funds to NEL and Ben Passey from the Department of Earth and Environmental Sciences (UM). We thank Ben Passey, Ian Winkelstern, and Drake Yarian for help with the triple oxygen isotope analyses and three reviewers whose constructive feedback improved the quality of this manuscript. Precipitation isotope data reported in this study are included in the supporting information and are available from the University of Utah Water Isotope Database (https://wateriso.utah.edu/waterisotopes/). The authors declare no conflicts of interest.

Figure 1. Spatial distribution of $\delta^{18}O_p$ and $\delta^{2}H_p$ observations in the central Andes (a) and this study (b). No previous studies have reported $\delta^{17}O_p$ from this region.

Figure 2. Mean 1989-2019 seasonal climatologies of the central Andes from ERA5 reanalysis data (Hersbach et al., 2020). Panels a and b show 850 hPa winds (vectors, m/s) and total daily precipitation (mm/day); c and d show 200 hPa winds (vectors, m/s) and total column rainwater (kg/m^2). The panels highlight summer (a and c) and winter (b and d) conditions. The geographic bounds of the central Andes are noted with a dotted box in b.

Figure 3. Semimonthly precipitation (colored by site) $\delta^{18}O$ versus $\delta^{2}H$ (a) and $\delta'^{18}O$ versus $\delta'^{17}O$ (b) with respect to the $\delta^{18}O$-$\delta^{2}H$ (Craig, 1961) and $\delta'^{18}O$-$\delta'^{17}O$ (Luz and Barkan, 2010) meteoric water lines, respectively. Panel b contains a subset of 32 samples from panel a.

Figure 4. Timeseries of semimonthly $\delta^{18}O_p$ (‰; a, b) and d-excess$_p$ (‰; c, d) from June 2016 through May 2019. Gray vertical bars indicate the rainy season (DJFM). For clarity, the data are separated into Eastern and Altiplano sites (a, c) and Western sites (b, d) and are colored by site location. Eastern and Altiplano sites received dry season precipitation; western sites typically did not. Missing data indicate rain did not fall during the collection period or the observer did not collect a sample.

Figure 5. Elevation profile along the A-B-C transect (a) and spatiotemporal variability of average amount-weighted rainy season $\delta^{18}O_p$ (b) and d-excess$_p$ (c) in southern Peru. Blue sites fall on or near the elevation profile; an elevation profile through the yellow sites is not shown, but the dominant topographical features through these sites are the same as those along the A-B-C transect. In b and c, the filled circles represent the multiyear average $\delta^{18}O_p$ and d-excess$_p$ values, respectively; the open symbols show data from 2017 (square), 2018 (diamond), and 2019 (triangle). Relatively invariant d-excess$_p$ values and an inverse elevation-$\delta^{18}O_p$ relationship point to Rayleigh distillation on both flanks from eastern and western-derived air masses.

Figure 6. Scatterplots of central Andean amount-weighted wet season $\delta^{18}O_p$, d-excess$_p$, and $\Delta'^{17}O$ variation with elevation (a, d, g), MAP (b, e, h), and latitude (c, f, i). In panels a through f, color differentiates $\delta^{18}O_p$ references, the solid black line shows the best fit linear regression through data from all studies, and the dotted line shows the best fit linear regression through data from this study. In panels g through i, shape differentiates references and color differentiates water type.

Figure 7. Scatterplots of $\delta'^{18}O$ versus $\Delta'^{17}O$ (a), $\delta^{18}O$ versus d-excess (b), and d-excess versus $\Delta'^{17}O$ (c) from this study (filled circles) and published precipitation (open circles) and surface waters (open diamonds) in the tropics and mid-latitudes. The open black diamonds show surface water data from the central Andes (Aron et al., 2021; Surma et al., 2018; Voigt et al., 2021). The open gray diamonds show surface water data from locations other than the central Andes (Affolter et al., 2015; Bergel et al., 2020; Bershaw et al., 2020; Gázquez et al., 2017; Li et al., 2017; Luz & Barkan, 2010; Nava-Fernandez et al., 2020; Passey & Ji, 2019; Surma, et al., 2015; Tian et al., 2021). The open circles show precipitation data (Affolter et al., 2015; Gázquez et al., 2017; Landais et al., 2010; Luz & Barkan, 2010; He et al., 2021; Surma et al., 2018; Tian et al., 2021; Tian & Wang, 2019; Uechi & Uemura, 2019). Error bars on $\Delta'^{17}O$ show the standard

deviation of multiple replicate analyses of each sample. There are more points in a than b or c because some published $\Delta'^{17}O$ studies do not include δ^2H data.

Figure 8. Timeseries of eastern (filled symbols) and western (open symbols) moisture flux ratios at San Gaban (a), Santo Tomas (b), Ayaviri (c), Cotahuasi (d), Ubinas (e), Majes (f), and Moquegua (g). The points represent the ratio of eastern versus western moisture at each site determined from atmospheric back trajectories and the Sodemann et al. (2008) humidity tracer. The yellow points were calculated from trajectories initiated on every day of the study period; the blue points were calculated with trajectories only from rainy days only. Gray vertical bars indicate the DJF rainy seasons.

Figure 9. Timeseries of monthly $\delta^{18}O_p$ (a), d-excess$_p$ (b), and precipitation (c) from this study (circles), Fiorella et al., 2015a (triangles), and Guy et al., 2019 (squares) colored by site-specific elevation. Vertical gray bars mark the DJFM rainy season.

References

Aceituno, P. (1988). On the Functioning of the Southern Oscillation in the South American Sector. Part 1: Surface Climate. *Monthly Weather Review*, *116*, 505–524.

Aemisegger, F., Pfahl, S., Sodemann, H., Lehner, I., Seneviratne, S. I., & Wernli, H. (2014). Deuterium excess as a proxy for continental moisture recycling and plant transpiration. *Atmospheric Chemistry and Physics*, *14*(8), 4029–4054. https://doi.org/10.5194/acp-14-4029-2014

Affolter, S., Häuselmann, A. D., Fleitmann, D., Häuselmann, P., & Leuenberger, M. (2015). Triple isotope (δD, $\delta^{17}O$, $\delta^{18}O$) study on precipitation, drip water and speleothem fluid inclusions for a Western Central European cave (NW Switzerland). *Quaternary Science Reviews*, *127*, 73–89. https://doi.org/10.1016/j.quascirev.2015.08.030

Aggarwal, P. K., Romatschke, U., Araguas-Araguas, L., Belachew, D., Longstaffe, F. J., Berg, P., et al. (2016). Proportions of convective and stratiform precipitation revealed in water isotope ratios. *Nature Geoscience*, *9*(8), 624–629. https://doi.org/10.1038/ngeo2739

Ampuero, A., Stríkis, N. M., Apaéstegui, J., Vuille, M., Novello, V. F., Espinoza, J. C., et al. (2020). The Forest Effects on the Isotopic Composition of Rainfall in the Northwestern Amazon Basin. *Journal of Geophysical Research: Atmospheres*, *125*(4), 1–16. https://doi.org/10.1029/2019jd031445

Aravena, R., Suzuki, O., Pena, H., Pollastri, A., Fuenzalida, H., & Grilli, A. (1999). Isotopic composition and origin of the precipitation in Northern Chile. *Applied Geochemistry*, *14*(4), 411–422. https://doi.org/10.1016/S0883-2927(98)00067-5

Aron, P. G., Levin, N. E., Beverly, E. J., Huth, T. E., Passey, B. H., Pelletier, E. M., et al. (2021). Triple oxygen isotopes in the water cycle. *Chemical Geology*, *565*, 120026. https://doi.org/10.1016/j.chemgeo.2020.120026

Baker, L., Franchi, I. A., Maynard, J., Wright, I. P., & Pillinger, C. T. (2002). A Technique for the Determination of $^{18}O/^{16}O$ and $^{17}O/^{16}O$ Isotopic Ratios in Water from Small Liquid and Solid Samples. *Analytical Chemistry*, *74*(7), 1665–1673. https://doi.org/10.1021/ac010509s

Barkan, E., & Luz, B. (2005). High precision measurements of $^{17}O/^{16}O$ and $^{18}O/^{16}O$ ratios in H_2O. *Rapid Communications in Mass Spectrometry*, *19*(24), 3737–3742. https://doi.org/10.1002/rcm.2250

Barkan, E., & Luz, B. (2007). Diffusivity fractionations of $H_2{}^{16}O/H_2{}^{17}O$ and $H_2{}^{16}O/H_2{}^{18}O$ in air

and their implications for isotope hydrology. *Rapid Communications in Mass Spectrometry*, *21*, 2999–3005. https://doi.org/10.1002/rcm.3180

Bergel, S. J., Barkan, E., Stein, M., & Affek, H. P. (2020). Carbonate $^{17}O_{excess}$ as a paleo-hydrology proxy: Triple oxygen isotope fractionation between H_2O and biogenic aragonite, derived from freshwater mollusks. *Geochimica et Cosmochimica Acta*, *275*, 36–47. https://doi.org/10.1016/j.gca.2020.02.005

Bershaw, J., Hansen, D. D., & Schauer, A. J. (2020). Deuterium excess and ^{17}O-excess variability in meteoric water across the Pacific Northwest, USA. *Tellus, Series B: Chemical and Physical Meteorology*, *72*(1), 1–17. https://doi.org/10.1080/16000889.2020.1773722

Bird, B. W., Abbott, M. B., Vuille, M., Rodbell, D. T., Stansell, N. D., & Rosenmeier, M. F. (2011). A 2,300-year-long annually resolved record of the South American summer monsoon from the Peruvian Andes. *Proceedings of the National Academy of Sciences*, *108*(21), 8583–8588. https://doi.org/10.1073/pnas.1003719108

Blossey, P. N., Kuang, Z., & Romps, D. M. (2010). Isotopic composition of water in the tropical tropopause layer in cloud-resolving simulations of an idealized tropical circulation. *Journal of Geophysical Research Atmospheres*, *115*(24), 1–23. https://doi.org/10.1029/2010JD014554

Bolot, M., Legras, B., & Moyer, E. J. (2013). Modelling and interpreting the isotopic composition of water vapour in convective updrafts. *Atmospheric Chemistry and Physics*, *13*(16), 7903–7935. https://doi.org/10.5194/acp-13-7903-2013

Bony, S., Risi, C., & Vimeux, F. (2008). Influence of convective processes on the isotopic composition ($\delta^{18}O$ and δD) of precipitation and water vapor in the tropics: 1. Radiative-convective equilibrium and Tropical Ocean-Global Atmosphere-Coupled Ocean-Atmosphere Response Experiment (TOGA-COARE). *Journal of Geophysical Research Atmospheres*, *113*(19), 1–21. https://doi.org/10.1029/2008JD009942

Bowen, G. J., Cai, Z., Fiorella, R. P., & Putman, A. L. (2019). Isotopes in the Water Cycle: Regional- to Global-Scale Patterns and Applications. *Annual Reviews*, *47*, 453–479. https://doi.org/10.1146/annurev-earth-053018- 060220

Bowen, G. J., & Wilkinson, B. H. (2002). Spatial distribution of $\delta^{18}O$ in meteoric precipitation. *Geology*, *30*(4), 315–318.

Craig, H. (1961). Isotopic Variations in Meteoric Waters. *Science*, *133*(3465), 1702–1703. https://doi.org/10.1126/science.133.3465.1702

Criss, R. E. (1999). *Principles of Stable Isotope Distribution*. New York: Oxford University Press.

Dansgaard, W. (1964). Stable isotopes in precipitation. *Tellus*, *16*(4), 436–468. https://doi.org/10.3402/tellusa.v16i4.8993

Draxler, R. R., & Hess, G. D. (1998). An overview of the HYSPLIT_4 modelling system for trajectories, dispersion and deposition. *Australian Meteorological Magazine*, *47*(4), 295–308.

Dütsch, M., Pfahl, S., & Sodemann, H. (2017). The impact of nonequilibrium and equilibrium fractionation on two different deuterium excess definitions. *Journal of Geophysical Research: Atmospheres*, *122*(23), 12,732-12,746. https://doi.org/10.1002/2017JD027085

Fiorella, R. P., Poulsen, C. J., & Matheny, A. M. (2018). Seasonal Patterns of Water Cycling in a Deep, Continental Mountain Valley Inferred From Stable Water Vapor Isotopes. *Journal of Geophysical Research: Atmospheres*, *123*(14), 7271–7291. https://doi.org/10.1029/2017JD028093

Fiorella, R. P., Poulsen, C. J., Zolá, R. S. P., Barnes, J. B., Tabor, C. R., & Ehlers, T. A. (2015a). Spatiotemporal variability of modern precipitation $\delta^{18}O$ in the central Andes and implications for paleoclimate and paleoaltimetry estimates. *Journal of Geophysical Research: Atmospheres*, *120*, 1–27. https://doi.org/10.1002/2014JD022893

Fiorella, R. P., Poulsen, C. J., Pillco, R. S., Jeffery, M. L., & Ehlers, T. A. (2015b). Modern and long-term evaporation of central Andes surface waters suggests paleo archives underestimate Neogene elevations. *Earth and Planetary Science Letters*, *432*, 59–72. https://doi.org/10.1016/j.epsl.2015.09.045

Friedman, I., Smith, G. I., Gleason, J. D., Warden, A., & Harris, J. M. (1992). Stable Isotope Composition of Waters in Southeastern California 1. Modern Precipitation. *Journal of Geophysical Research*, *97*(D5), 5795–5812.

Fritz, P., Suzuki, O., Silva, C., & Salati, E. (1981). Isotope hydrology of groundwaters in the Pampa del Tamarugal, Chile. *Journal of Hydrology*, *53*(1–2), 161–184. https://doi.org/10.1016/0022-1694(81)90043-3

Froehlich, K., Kralik, M., Papesch, W., Rank, D., Scheifinger, H., & Stichler, W. (2008). Deuterium excess in precipitation of Alpine regions – moisture recycling. *Isotopes in Environmental and Health Studies*, *44*(1), 61–70.

Galewsky, J., Steen-Larsen, H. C., Field, R. D., Worden, J., Risi, C., & Schneider, M. (2016). Stable isotopes in atmospheric water vapor and applications to the hydrologic cycle. *Reviews of Geophysics*, *54*(4), 809–865. https://doi.org/10.1002/2015RG000512

Garreaud, R. D. (2018). A plausible atmospheric trigger for the 2017 coastal El Niño. *International Journal of Climatology*, *38*(January 2017), e1296–e1302. https://doi.org/10.1002/joc.5426

Garreaud, R. D., Rutllant, J. A., & Fuenzalida, H. (2002). Coastal lows along the subtropical west coast of South America: Mean structure and evolution. *Monthly Weather Review*, *130*(1), 75–88. https://doi.org/10.1175/1520-0493(2002)130<0075:CLATSW>2.0.CO;2

Garreaud, R. D., Vuille, M., Compagnucci, R., & Marengo, J. (2009). Present-day South American climate. *Palaeogeography, Palaeoclimatology, Palaeoecology*, *281*(3–4), 180–195. https://doi.org/10.1016/j.palaeo.2007.10.032

Garreaud, R. (2009). The Andes climate and weather. *Advances In Geosciences*, *7*, 1–9. https://doi.org/10.5194/adgeo-22-3-2009

Garreaud, R. D., Vuille, M., Clement, A. (2003). The Climate of the Altiplano: Observed current conditions and mechanisms of past changes. *Palaeogeography, Palaeoclimatology, Palaeoecology*, *195*(5–22), 180–195. https://doi.org/10.1016/S0031-0182(03)00269-4

Garreaud, R. D. (1999). Multiscale Analysis of the Summertime Precipitation over the Central Andes. *Monthly Weather Review*, *127*(5), 901–921. https://doi.org/10.1175/1520-0493(1999)127<0901:MAOTSP>2.0.CO;2

Garzione, C. N., Molnar, P., Libarkin, J. C., & MacFadden, B. J. (2006). Rapid late Miocene rise of the Bolivian Altiplano: Evidence for removal of mantle lithosphere. *Earth and Planetary Science Letters*, *241*(3–4), 543–556. https://doi.org/10.1016/j.epsl.2005.11.026

Garzione, C. N., McQuarrie, N., Perez, N. D., Ehlers, T. A., Beck, S. L., Kar, N., et al. (2017). Tectonic Evolution of the Central Andean Plateau and Implications for the Growth of Plateaus. *Annual Review of Earth and Planetary Sciences*, *45*(1), 529–559. https://doi.org/10.1146/annurev-earth-063016-020612

Gat, J. (1996). Oxygen and hydrogen isotopes in the hydrologic cycle. *Annual Review of Earth and Planetary Sciences*, *24*, 225–262. https://doi.org/10.1146/annurev.earth.24.1.225

Gázquez, F., Calaforra, J. M., Evans, N. P., & Hodell, D. A. (2017). Using stable isotopes ($\delta^{17}O$, $\delta^{18}O$ and δD) of gypsum hydration water to ascertain the role of water condensation in the formation of subaerial gypsum speleothems. *Chemical Geology*, *452*, 34–46. https://doi.org/10.1016/j.chemgeo.2017.01.021

Giovannettone, J. P., & Barros, A. P. (2009). Probing Regional Orographic Controls of Precipitation and Cloudiness in the Central Andes Using Satellite Data. *Journal of Hydrology*, *10*, 167–182. https://doi.org/10.1175/2008JHM973.1

Gonfiantini, R. (1978). Standards for stable isotope measurements in natural compounds. *Nature*, *271*, 534–536. https://doi.org/10.1038/271534a0

Gonfiantini, R., Roche, M. A., Olivry, J. C., Fontes, J. C., & Zuppi, G. M. (2001). The altitude effect on the isotopic composition of tropical rains. *Chemical Geology*, *181*, 147–167. https://doi.org/10.1016/S0009-2541(01)00279-0

Gonfiantini, R., Wassenaar, L. I., Araguas-Araguas, L., & Aggarwal, P. K. (2018). A unified Craig-Gordon isotope model of stable hydrogen and oxygen isotope fractionation during fresh or saltwater evaporation. *Geochimica et Cosmochimica Acta*, *235*, 224–236. https://doi.org/10.1016/j.gca.2018.05.020

Gröning, M., Lutz, H. O., Roller-Lutz, Z., Kralik, M., Gourcy, L., & Pöltenstein, L. (2012). A simple rain collector preventing water re-evaporation dedicated for $\delta^{18}O$ and $\delta^{2}H$ analysis of cumulative precipitation samples. *Journal of Hydrology*, *449*, 195–200. https://doi.org/10.1016/j.jhydrol.2012.04.041

Guy, H., Seimon, A., Perry, L. B., Konecky, B. L., Rado, M., Andrade, M., et al. (2019). Subseasonal Variations of Stable Isotopes in Tropical Andean Precipitation. *Journal of Hydrometeorology*, *20*(5), 915–933. https://doi.org/10.1175/JHM-D-18-0163.1

Hardy, D. R., Vuille, M., & Bradley, R. S. (2003). Variability of snow accumulation and isotopic composition on Nevado Sajama, Bolivia. *Journal of Geophysical Research D: Atmospheres*, *108*(22), 1–10. https://doi.org/10.1029/2003jd003623

He, S., Jackisch, D., Samanta, D., Yi, P. K. Y., Liu, G., Wang, X., & Goodkin, N. F. (2021). Understanding Tropical Convection Through Triple Oxygen Isotopes of Precipitation From the Maritime Continent. *Journal of Geophysical Research: Atmospheres*, *126*(4), 1–14. https://doi.org/10.1029/2020JD033418

Herrera, C., Gamboa, C., Custodio, E., Jordan, T., Godfrey, L., Jódar, J., et al. (2018). Groundwater origin and recharge in the hyperarid Cordillera de la Costa, Atacama Desert, northern Chile. *Science of the Total Environment*, *624*, 114–132. https://doi.org/10.1016/j.scitotenv.2017.12.134

Hersbach, H., Bell, B., Berrisford, P., Hirahara, S., Andras, H., Joaquın, M.-S., et al. (2020). The ERA5 Global Reanalysis. *Quarterly Journal of the Royal Meteorological Society*, *146(730)*, 1999-2049. https://doi.org/10.1002/qj.3803.

Herwartz, D., Surma, J., Voigt, C., Assonov, S., & Staubwasser, M. (2017). Triple oxygen isotope systematics of structurally bonded water in gypsum. *Geochimica et Cosmochimica Acta*, *209*, 254–266. https://doi.org/10.1016/j.gca.2017.04.026

Hulston, J. R., & Thode, H. G. (1965). Variations in the S^{33}, S^{34}, and S^{36} Contents of Meteorites and Their Relation to Chemical and Nuclear Effects. *Journal of Geophysical Research*, *70*(14), 3475–3484.

Hurley, J. V., Vuille, M., & Hardy, D. R. (2019). On the Interpretation of the ENSO Signal Embedded in the Stable Isotopic Composition of Quelccaya Ice Cap, Peru. *Journal of Geophysical Research: Atmospheres*, *124*(1), 131–145.

https://doi.org/10.1029/2018JD029064

Insel, N., Poulsen, C. J., & Ehlers, T. A. (2010). Influence of the Andes Mountains on South American moisture transport, convection, and precipitation. *Climate Dynamics*, *35*, 1477–1492. https://doi.org/10.1007/s00382-009-0637-1

Jeffery, M. L., Poulsen, C. J., & Ehlers, T. A. (2012). Impacts of Cenozoic global cooling, surface uplift, and an inland seaway on South American paleoclimate and precipitation $\delta^{18}O$. *Bulletin of the Geological Society of America*, *124*(3–4), 335–351. https://doi.org/10.1130/B30480.1

Jouzel, J., & Merlivat, L. (1984). Deuterium and Oxygen 18 in Precipitation: Modeling of the Isotopic Effects During Snow Formation. *Journal of Geophysical Research*, *89*(D7), 11749–11757. https://doi.org/10.1029/JD089iD07p11749

Konecky, B. L., Noone, D. C., & Cobb, K. M. (2019). The Influence of Competing Hydroclimate Processes on Stable Isotope Ratios in Tropical Rainfall. *Geophysical Research Letters*, *46*, 1622–1633. https://doi.org/10.1029/2018GL080188

Kumar, S., Vidal, Y., Moya-Álvarez, A. S., & Martínez-Castro, D. (2019). Effect of the surface wind flow and topography on precipitating cloud systems over the Andes and associated Amazon basin: GPM observations. *Atmospheric Research*, *225*(February), 193–208. https://doi.org/10.1016/j.atmosres.2019.03.027

Kurita, N. (2013). Water isotopic variability in response to mesoscale convective system over the tropical ocean. *Journal of Geophysical Research Atmospheres*, *118*(18), 10,376-10,390. https://doi.org/10.1002/jgrd.50754

Landais, A., Barkan, E., Yakir, D., & Luz, B. (2006). The triple isotopic composition of oxygen in leaf water. *Geochimica et Cosmochimica Acta*, *70*(16), 4105–4115. https://doi.org/10.1016/j.gca.2006.06.1545

Landais, A., Risi, C., Bony, S., Vimeux, F., Descroix, L., Falourd, S., & Bouygues, A. (2010). Combined measurements of $^{17}O_{excess}$ and d-excess in African monsoon precipitation: Implications for evaluating convective parameterizations. *Earth and Planetary Science Letters*, *298*(1–2), 104–112. https://doi.org/10.1016/j.epsl.2010.07.033

Lechler, A. R., & Niemi, N. A. (2011). Controls on the spatial variability of modern meteoric $\delta^{18}O$: Empirical constraints from the western U.S. and East Asia and implications for stable isotope studies. *American Journal of Science*, *311*(8), 664–700. https://doi.org/10.2475/08.2011.02

Legates, D. R., & Willmott, C. J. (1990a). Mean Seasonal and Spatial Variability in Gauge-Corrected, Global Precipitation. *International Journal of Climatology*, *10*, 111–127.

Legates, D. R., & Willmott, C. J. (1990b). Mean seasonal and spatial variability in global surface air temperature. *Theoretical and Applied Climatology*, *41*(1–2), 11–21. https://doi.org/10.1007/BF00866198

Lenters, J. D., & Cook, K. H. (1997). On the Origin of the Bolivian High and Related Circulation Features of the South American Climate. *Journal of the Atmospheric Sciences*, *54*(5), 656–678. https://doi.org/10.1175/1520-0469(1997)054<0656:OTOOTB>2.0.CO;2

Li, S., Levin, N. E., Soderberg, K., Dennis, K. J., & Caylor, K. K. (2017). Triple oxygen isotope composition of leaf waters in Mpala, central Kenya. *Earth and Planetary Science Letters*, *468*, 38–50. https://doi.org/10.1016/j.epsl.2017.02.015

Liotta, M., Favara, R., & Valenza, M. (2006). Isotopic composition of the precipitations in the central Mediterranean: Origin marks and orographic precipitation effects. *Journal of Geophysical Research Atmospheres*, *111*(19), 1–12. https://doi.org/10.1029/2005JD006818

Luz, B., & Barkan, E. (2010). Variations of $^{17}O/^{16}O$ and $^{18}O/^{16}O$ in meteoric waters. *Geochimica et Cosmochimica Acta*, *74*(22), 6276–6286. https://doi.org/10.1016/j.gca.2010.08.016

Matsuhisa, Y., Goldsmith, J. R., & Clayton, R. N. (1978). Mechanisms of hydrothermal crystallization of quartz at 250°C and 15 kbar. *Geochimica et Cosmochimica Acta*, *42*(2), 173–182. https://doi.org/10.1016/0016-7037(78)90130-8

Meijer, H. A. J., & Li, W. J. (1998). The Use of Electrolysis for Accurate $\delta^{17}O$ and $\delta^{18}O$ Isotope Measurements in Water. *Isotopes in Evironmental Health Studies*, *34*(4), 349–369. https://doi.org/10.1080/10256019808234072

Miller, M. F. (2002). Isotopic fractionation and the quantification of ^{17}O anomalies in the oxygen three-isotope system: an appraisal and geochemical significance. *Geochimica et Cosmochimica Acta*, *66*(11), 1881–1889. Retrieved from http://www.sciencedirect.com/science/article/pii/S0016703702008323

Moore, M., Kuang, Z., & Blossey, P. N. (2014). A moisture budget perspective of the amount effect. *Geophysical Research Letters*, *41*(4), 1329–1335. https://doi.org/10.1002/2013GL058302

National Weather Service, Climate Prediction Center: https://origin.cpc.ncep.noaa.gov/products/analysis_monitoring/ensostuff/ONI_v5.php, Accessed June 1, 2020

Nava-Fernandez, C., Hartland, A., Gázquez, F., Kwiecien, O., Marwan, N., Fox, B., et al. (2020). Pacific climate reflected in Waipuna Cave drip water hydrochemistry. *Hydrology and Earth System Sciences*, *24*(6), 3361–3380. https://doi.org/10.5194/hess-24-3361-2020

Passey, B. H., Hu, H., Ji, H., Montanari, S., Li, S., Henkes, G. A., & Levin, N. E. (2014). Triple oxygen isotopes in biogenic and sedimentary carbonates. *Geochimica et Cosmochimica Acta*, *141*, 1–25. https://doi.org/10.1016/j.gca.2014.06.006

Passey, B. H., & Ji, H. (2019). Triple oxygen isotope signatures of evaporation in lake waters and carbonates: A case study from the western United States. *Earth and Planetary Science Letters*, *518*, 1–12. https://doi.org/10.1016/j.epsl.2019.04.026

Pattnayak, K. C., Tindall, J. C., Brienen, R. J. W., Barichivich, J., & Gloor, E. (2019). Can We Detect Changes in Amazon Forest Structure Using Measurements of the Isotopic Composition of Precipitation? *Geophysical Research Letters*, *46*(24), 14807–14816. https://doi.org/10.1029/2019GL084749

Peng, Q., Xie, S. P., Wang, D., Zheng, X. T., & Zhang, H. (2019). Coupled ocean-atmosphere dynamics of the 2017 extreme coastal El Niño. *Nature Communications*, *10*(1), 1–10. https://doi.org/10.1038/s41467-018-08258-8

Pfahl, S., & Sodemann, H. (2014). What controls deuterium excess in global precipitation? *Climate of the Past*, *10*(2), 771–781. https://doi.org/10.5194/cp-10-771-2014

Pillco Zolá, R., Bengtsson, L., Berndtsson, R., Martí-Cardona, B., Satgé, F., Timouk, F., et al. (2019). Modelling Lake Titicaca's daily and monthly evaporation. *Hydrology and Earth System Sciences*, *23*(2), 657–668. https://doi.org/10.5194/hess-23-657-2019

Poulsen, C. J., Ehlers, T. A., & Insel, N. (2010). Onset of Convective Rainfall During Gradual Late Miocene Rise of the Central Andes. *Science*, *328*(5977), 490–493. https://doi.org/10.1126/science.1185078

Quinn, W. H., & Neal, V. T. (1987). El Nino Occurrences Over the Past Four and a Half Centuries. *Journal of Geophysical Research*, *92*(C13), 14,449-14,461.

Rech, J. A., Currie, B. S., Jordan, T. E., Riquelme, R., Lehmann, S. B., Kirk-Lawlor, N. E., et al. (2019). Massive middle Miocene gypsic paleosols in the Atacama Desert and the formation

of the Central Andean rain-shadow. *Earth and Planetary Science Letters*, *506*, 184–194. https://doi.org/10.1016/j.epsl.2018.10.040

Risi, C., Landais, A., Winkler, R., & Vimeux, F. (2013). Can we determine what controls the spatio-temporal distribution of d-excess and ^{17}O-excess in precipitation using the LMDZ general circulation model? *Climate of the Past*, *9*(5), 2173–2193. https://doi.org/10.5194/cp-9-2173-2013

Risi, C., Bony, S., & Vimeux, F. (2008). Influence of convective processes on the isotopic composition ($\delta^{18}O$ and δD) of precipitation and water vapor in the tropics: 2. Physical interpretation of the amount effect. *Journal of Geophysical Research Atmospheres*, *113*(19), 1–12. https://doi.org/10.1029/2008JD009943

Rodwell, M. J., & Hoskins, B. J. (2001). Subtropical anticyclones and summer monsoons. *Journal of Climate*, *14*(15), 3192–3211. https://doi.org/10.1175/1520-0442(2001)014<3192:SAASM>2.0.CO;2

Romatschke, U., & Houze, R. A. (2010). Extreme summer convection in South America. *Journal of Climate*, *23*(14), 3761–3791. https://doi.org/10.1175/2010JCLI3465.1

Rozanski, K., Araguás-Araguás, L., & Gonfiantini, R. (1993). Isotopic Patterns in Modern Global Precipitation. In P. K. Swart, K. C. Lohmann, J. Mckenzie, & S. Savin (Eds.), *Climate change in continental isotopic records Geophysical Monograph Series, (Vol. 78)* (pp. 1–36). Washington, DC: American Geophysical Union. https://doi.org/10.1029/GM078p0001

Rutllant, J. A., Fuenzalida, H., & Aceituno, P. (2003). Climate dynamics along the arid northern coast of Chile: The 1997–1998 Dinámica del Clima de la Región de Antofagasta (DICLIMA) experiment. *Journal of Geophysical Research*, *108*(D17), 1–13. https://doi.org/10.1029/2002JD003357

Salati, E., Dall'Olio, A., Matsui, E., & Gat, J. R. (1979). Recycling of water in the Amazon Basin: An isotopic study. *Water Resources Research*, *15*(5), 1250–1258. https://doi.org/10.1029/WR015i005p01250

Samuels-Crow, K. E., Galewsky, J., Hardy, D. R., Sharp, Z. D., Worden, J., & Braun, C. (2014a). Upwind convective influences on the isotopic composition of atmospheric water vapor over the tropical Andes. *Journal Geophysical Research Atmospheres*, *119*, 7051–7063. https://doi.org/10.1002/2014JD021487.Received

Samuels-Crow, K. E., Galewsky, J., Sharp, Z. D., & Dennis, K. J. (2014b). Deuterium excess in subtropical free troposphere water vapor: Continuous measurements from the Chajnantor Plateau, northern Chile. *Geophysical Research Letters*, *41*(23), 8652–8659. https://doi.org/10.1002/2014GL062302

Schoenemann, S. W., Schauer, A. J., & Steig, E. J. (2013). Measurement of SLAP2 and GISP $\delta^{17}O$ and proposed VSMOW-SLAP normalization for $\delta^{17}O$ and $^{17}O_{excess}$. *Rapid Communications in Mass Spectrometry*, *27*(5), 582–590. https://doi.org/10.1002/rcm.6486

Scholl, M. A., Ingebritsen, S. E., Janik, C. J., & Kauahikaua, J. P. (1996). Use of precipitation and groundwater isotopes to interpret regional hydrology on a tropical volcanic island: Kilauea volcano area, Hawaii. *Water Resources Research*, *32*(12), 3525–3537.

Sodemann, H., Schwierz, C., & Wernli, H. (2008). Interannual variability of Greenland winter precipitation sources: Lagrangian moisture diagnostic and North Atlantic Oscillation influence. *Journal of Geophysical Research Atmospheres*, *113*(3), 1–17. https://doi.org/10.1029/2007JD008503

Spangenberg, J. E. (2012). Caution on the storage of waters and aqueous solutions in plastic

containers for hydrogen and oxygen stable isotope analysis. *Rapid Communications in Mass Spectrometry*, *26*, 2627–2636. https://doi.org/10.1002/rcm.6386

Sturm, C., Hoffmann, G., & Langmann, B. (2007). Simulation of the Stable Water Isotopes in Precipitation over South America: Comparing Regional to Global Circulation Models. *Journal of Climate*, *20*, 3730–3750. https://doi.org/10.1175/JCLI4194.1

Surma, J., Assonov, S., Herwartz, D., Voigt, C., & Staubwasser, M. (2018). The evolution of ^{17}O-excess in surface water of the arid environment during recharge and evaporation. *Scientific Reports*, *8*(1), 1–10. https://doi.org/10.1038/s41598-018-23151-6

Surma, J., Assonov, S., Bolourchi, M. J., & Staubwasser, M. (2015). Triple oxygen isotope signatures in evaporated water bodies from the Sistan Oasis, Iran. *Geophysical Research Letters*, *42*(20), 8456–8462. https://doi.org/10.1002/2015GL066475

Takahashi, K., & Martínez, A. G. (2019). The very strong coastal El Niño in 1925 in the far-eastern Pacific. *Climate Dynamics*, *52*(12), 7389–7415. https://doi.org/10.1007/s00382-017-3702-1

Tian, C., Jiao, W., Beysens, D., Farai Kaseke, K., Medici, M. G., Li, F., & Wang, L. (2021). Investigating the role of evaporation in dew formation under different climates using 17O-excess. *Journal of Hydrology*, *592*(December 2020), 125847. https://doi.org/10.1016/j.jhydrol.2020.125847

Tian, C., & Wang, L. (2019). Data Descriptor: Stable isotope variations of daily precipitation from 2014 – 2018 in the central United States. *Scientific Data*, *6*, 1–8. https://doi.org/10.1038/sdata.2019.18

Thompson, L. G., Davis, M. E., Mosley-Thompson, E., Beaudon, E., Porter, S. E., Kutuzov, S., et al. (2017). Impacts of Recent Warming and the 2015/2016 El Niño on Tropical Peruvian Ice Fields. *Journal Geophysical Research Atmospheres*, *122*, 688–701. https://doi.org/10.1002/2017JD026592

Uechi, Y., & Uemura, R. (2019). Dominant influence of the humidity in the moisture source region on the ^{17}O-excess in precipitation on a subtropical island. *Earth and Planetary Science Letters*, *513*, 20–28. https://doi.org/10.1016/j.epsl.2019.02.012

Valdivielso, S., Vázquez-Suñé, E., & Custodio, E. (2020). Origin and variability of oxygen and hydrogen isotopic composition of precipitation in the Central Andes: A review. *Journal of Hydrology*, *587*(December 2019), 124899. https://doi.org/10.1016/j.jhydrol.2020.124899

Vera, C., Baez, J., Douglas, M., Emmanuel, C. B., Marengo, J., Meitin, J., et al. (2006). The South American Low-Level Jet Experiment. *Bulletin of the American Meteorological Society*, *87*(1), 63–77. https://doi.org/10.1175/BAMS-87-1-63

Vimeux, F., Gallaire, R., Bony, S., Hoffmann, G., & Chiang, J. C. H. (2005). What are the climate controls on δD in precipitation in the Zongo Valley (Bolivia)? Implications for the Illimani ice core interpretation. *Earth and Planetary Science Letters*, *240*(2), 205–220. https://doi.org/10.1016/j.epsl.2005.09.031

Vimeux, F., Tremoy, G., Risi, C., & Gallaire, R. (2011). A strong control of the South American SeeSaw on the intra-seasonal variability of the isotopic composition of precipitation in the Bolivian Andes. *Earth and Planetary Science Letters*, *307*(1–2), 47–58. https://doi.org/10.1016/j.epsl.2011.04.031

Voigt, C., Herwartz, D., Dorador, C., & Staubwasser, M. (2021). Triple oxygen isotope systematics of evaporation and mixing processes in a dynamic desert lake system. *Hydrology and Earth System Sciences*, *25*(3), 1211–1228. https://doi.org/10.5194/hess-25-1211-2021

Vuille, M., Bradley, R. S., & Keimig, F. (2000). Climate variability in the Andes of Ecuador and its relation to tropical Pacific and Atlantic Sea Surface temperature anomalies. *Journal of Climate*, *13*(14), 2520–2535. https://doi.org/10.1175/1520-0442(2000)013<2520:CVITAO>2.0.CO;2

Vuille, M., Burns, S. J., Taylor, B. L., Cruz, F. W., Bird, B. W., Abbott, M. B., et al. (2012). A review of the South American monsoon history as recorded in stable isotopic proxies over the past two millennia. *Climate of the Past*, *8*(4), 1309–1321. https://doi.org/10.5194/cp-8-1309-2012

Vuille, M., & Werner, M. (2005). Stable isotopes in precipitation recording South American summer monsoon and ENSO variability: Observations and model results. *Climate Dynamics*, *25*(4), 401–413. https://doi.org/10.1007/s00382-005-0049-9

Worden, J., Noone, D., Bowman, K., Beer, R., Eldering, A., Fisher, B., et al. (2007). Importance of rain evaporation and continental convection in the tropical water cycle. *Nature*, *445*(7127), 528–532. https://doi.org/10.1038/nature05508

Young, E. D., Galy, A., & Nagahara, H. (2002). Kinetic and equilibrium mass-dependent isotope fractionation laws in nature and their geochemical and cosmochemical significance. *Geochimica et Cosmochimica Acta*, *66*(6), 1095–1104. https://doi.org/10.1016/S0016-7037(01)00832-8

Figure 1.

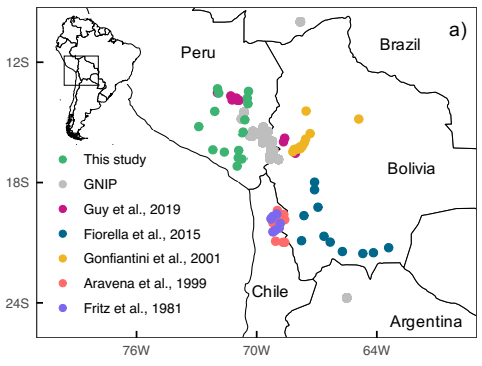

Precipitation collection stations (this study)

- San Gaban (SGN)
- Ollachea (OLL)
- Macusani (MAC)
- Ayaviri (AYV)
- Santo Tomas (SNT)
- Cuzco (CUZ)
- Calca (CAL)
- Pampahuta (PAM)
- Cotahuasi (COT)
- Ubinas (UBN)
- Carumas (CAR)
- Quinistaquillas (QUI)
- Arequipa (APQ)
- Moquegua (MOQ)
- Majes (MAJ)

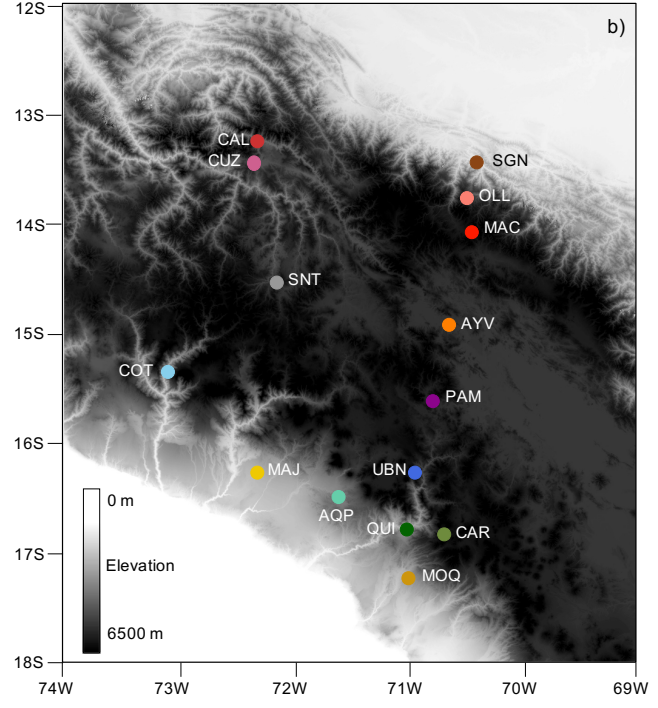

Figure 2.

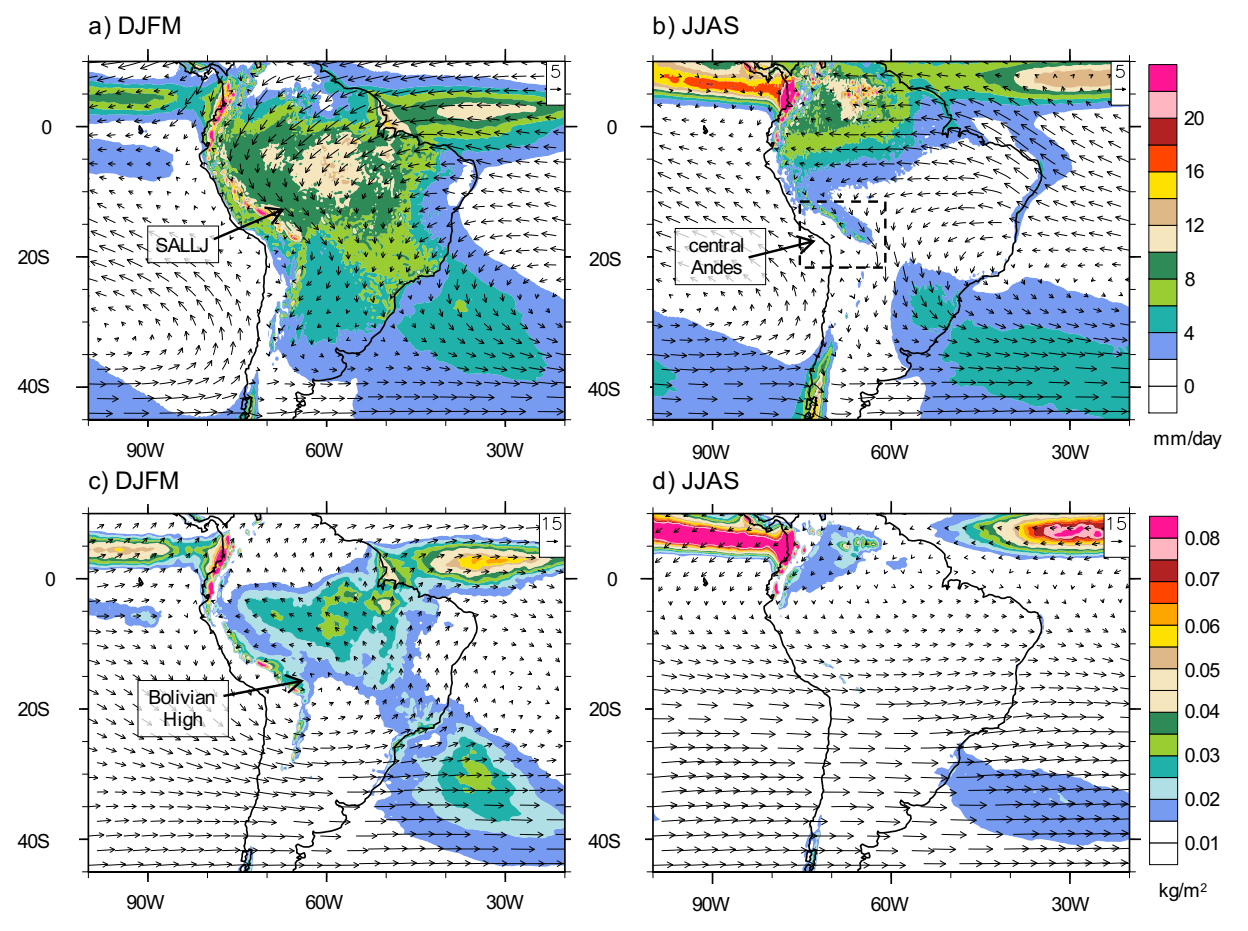
a) DJFM
b) JJAS
c) DJFM
d) JJAS
SALLJ
central Andes
Bolivian High
5
15
0
20S
40S
90W
60W
30W
20
16
12
8
4
0
mm/day
0.08
0.07
0.06
0.05
0.04
0.03
0.02
0.01
kg/m²

Figure 3.

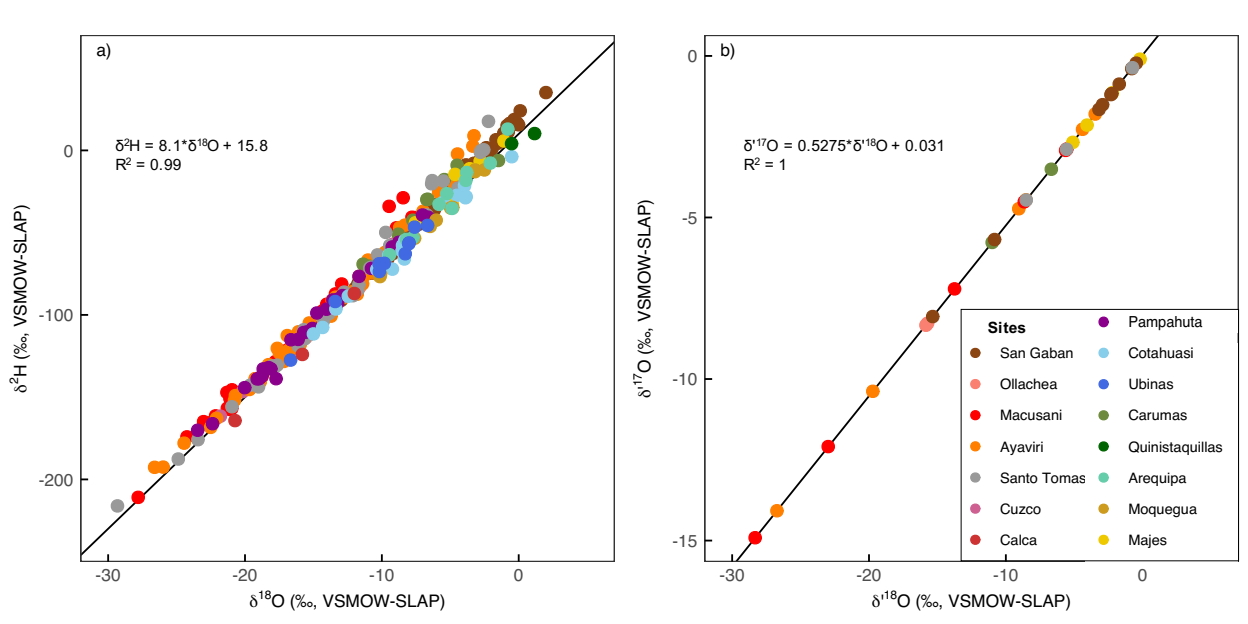
a)
δ²H = 8.1*δ¹⁸O + 15.8
R² = 0.99
δ²H (‰, VSMOW-SLAP)
δ¹⁸O (‰, VSMOW-SLAP)
0
-100
-200
-30
-20
-10
0
b)
δ¹⁷O = 0.5275*δ¹⁸O + 0.031
R² = 1
δ¹⁷O (‰, VSMOW-SLAP)
δ¹⁸O (‰, VSMOW-SLAP)
0
-5
-10
-15
Sites
San Gaban
Ollachea
Macusani
Ayaviri
Santo Tomas
Cuzco
Calca
Pampahuta
Cotahuasi
Ubinas
Carumas
Quinistaquillas
Arequipa
Moquegua
Majes

Figure 4.

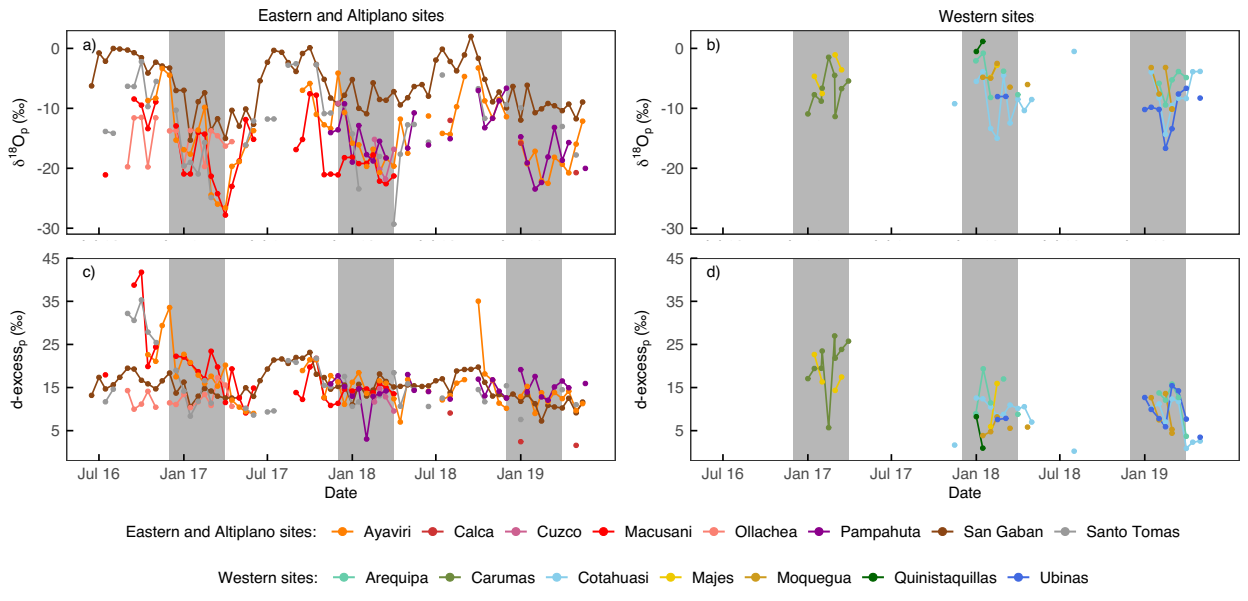
Eastern and Altiplano sites
Western sites
a)
b)
c)
d)
δ18Op (‰)
d-excessp (‰)
0
-10
-20
-30
45
35
25
15
5
Jul 16
Jan 17
Jul 17
Jan 18
Jul 18
Jan 19
Date
Eastern and Altiplano sites: Ayaviri Calca Cuzco Macusani Ollachea Pampahuta San Gaban Santo Tomas
Western sites: Arequipa Carumas Cotahuasi Majes Moquegua Quinistaquillas Ubinas

Figure 5.

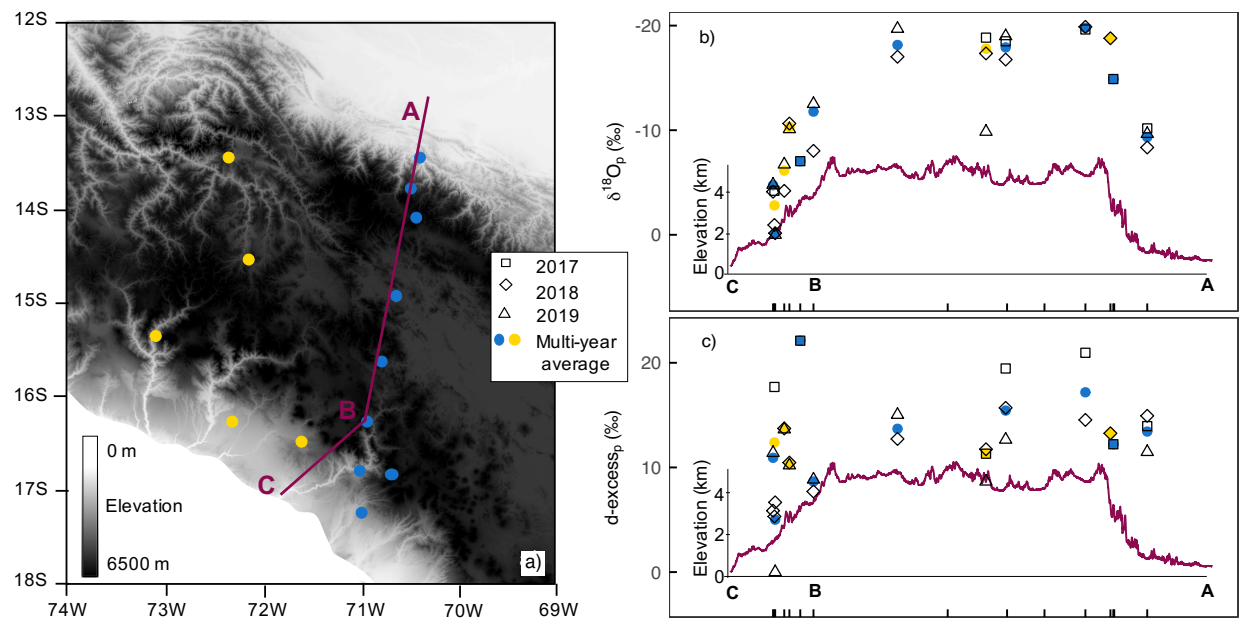
12S
13S
14S
15S
16S
17S
18S
74W
73W
72W
71W
70W
69W
A
B
C
0 m
Elevation
6500 m
a)
2017
2018
2019
Multi-year average
b)
$\delta^{18}O_p$ (‰)
-20
-10
0
Elevation (km)
4
2
0
C
B
A
c)
d-excess$_p$ (‰)
20
10
0

Figure 6.

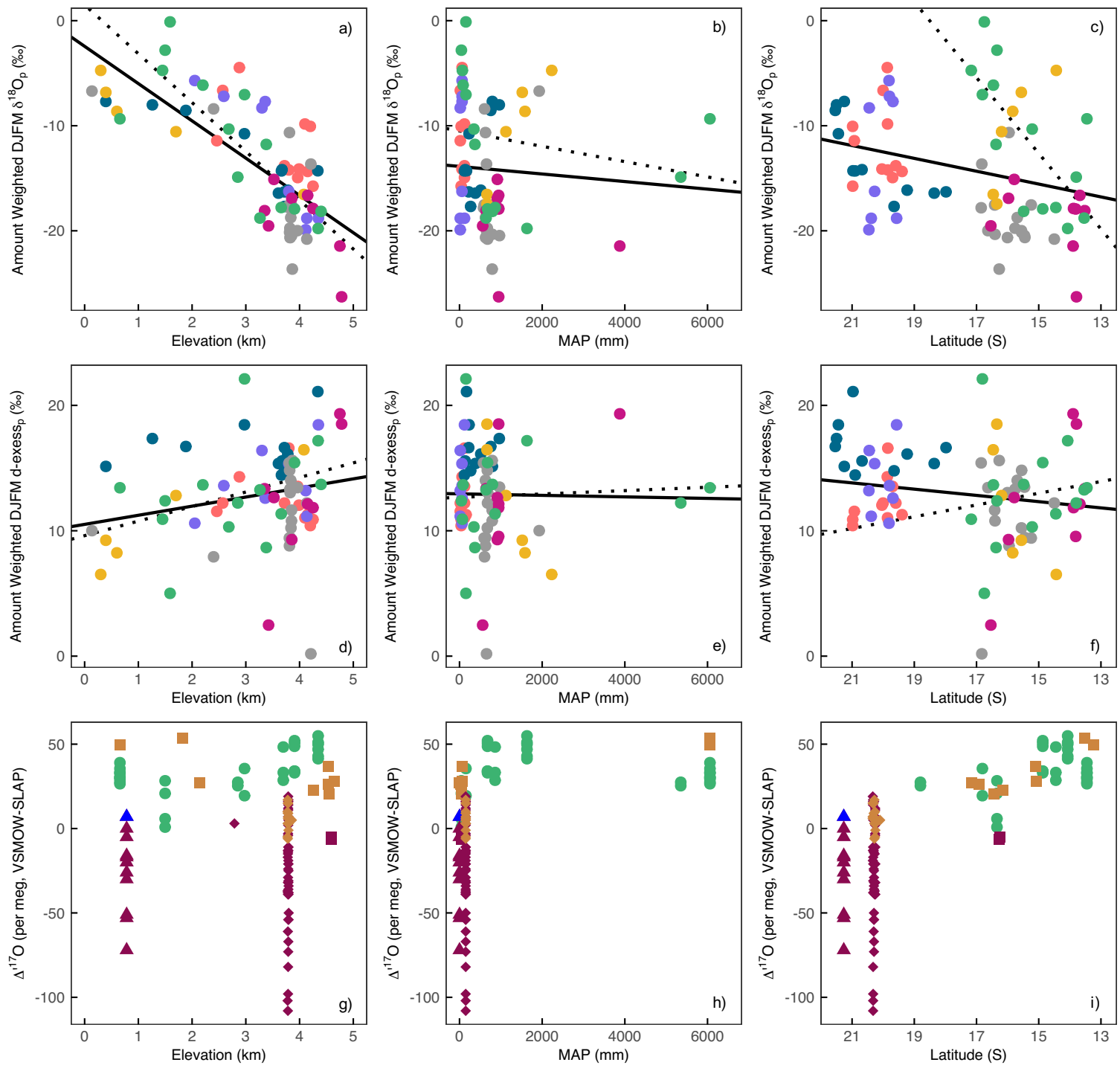
a)
b)
c)
d)
e)
f)
g)
h)
i)
Amount Weighted DJFM δ18Op (‰)
Amount Weighted DJFM d-excessp (‰)
Δ'17O (per meg, VSMOW-SLAP)
Elevation (km)
MAP (mm)
Latitude (S)
Reference
Aravena et al., 2001
Fiorella et al., 2015
Fritz et al., 1981
GNIP
Gonfiantini et al., 2001
Guy et al., 2019
This study
Water Type
Ground
Lake
Precipitation
Stream
Reference
Aron et al., 2021
Surma et al., 2018
This study
Voigt et al., 2021

Figure 7.

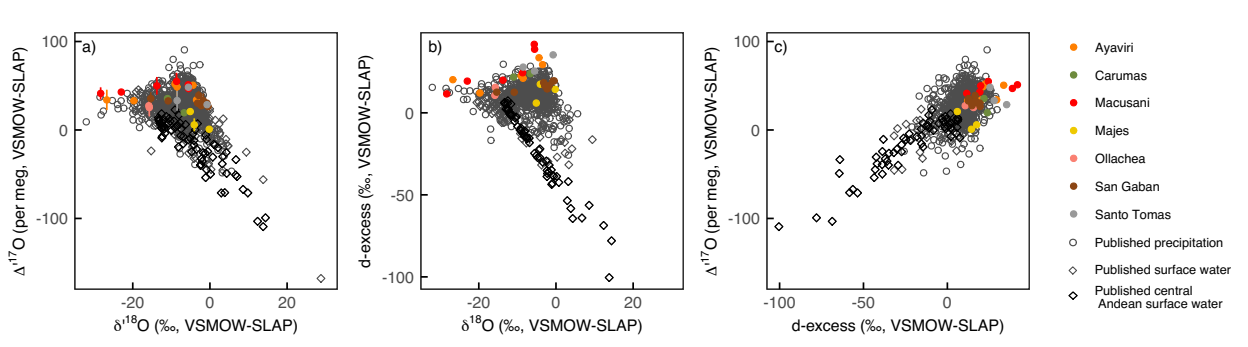
a)
b)
c)
100
0
-100
-20
0
20
-50
-100
-50
0
Δ'17O (per meg, VSMOW-SLAP)
δ'18O (‰, VSMOW-SLAP)
d-excess (‰, VSMOW-SLAP)
Ayaviri
Carumas
Macusani
Majes
Ollachea
San Gaban
Santo Tomas
Published precipitation
Published surface water
Published central Andean surface water

Figure 8.

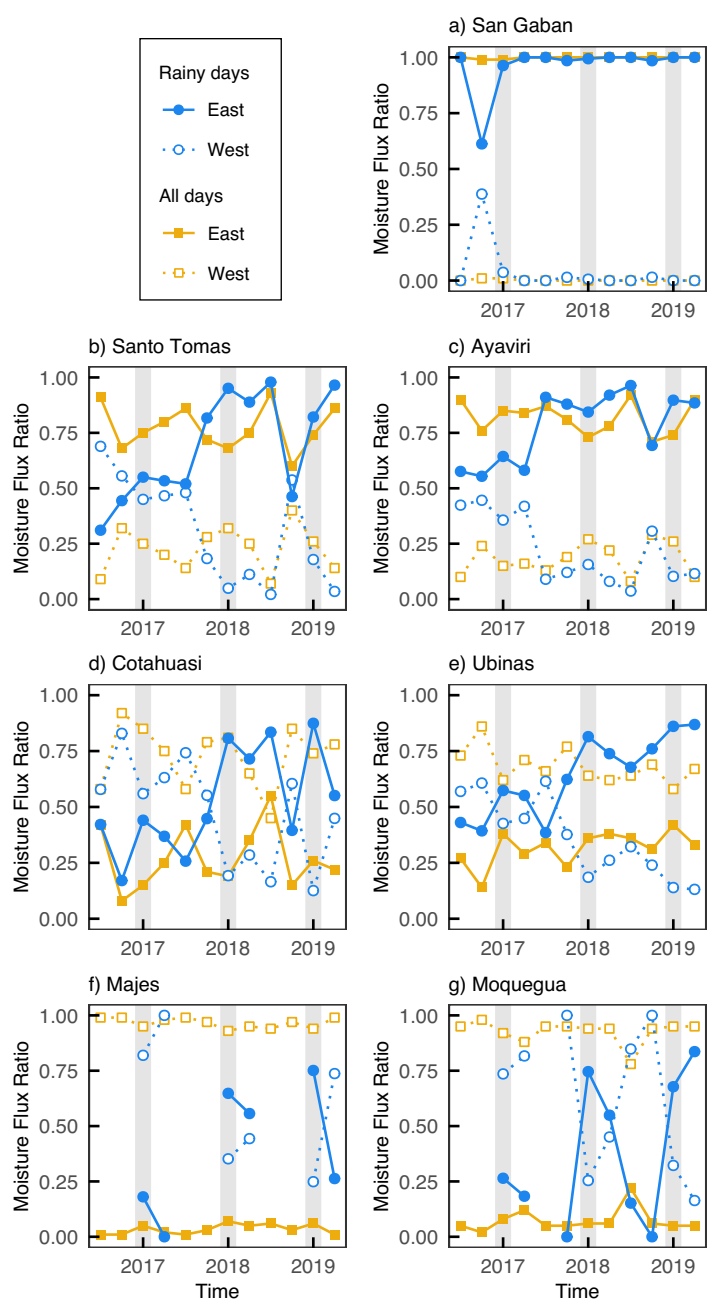
Rainy days
East
West
All days
East
West
a) San Gaban
b) Santo Tomas
c) Ayaviri
d) Cotahuasi
e) Ubinas
f) Majes
g) Moquegua
Moisture Flux Ratio
0.00
0.25
0.50
0.75
1.00
2017
2018
2019
Time

Figure 9.

a)
b)
c)
$\delta^{18}O_p$ (‰)
d-excess$_p$ (‰)
Precipitation (mm)
10
0
-10
-20
-30
40
30
20
10
0
1000
750
500
250
0
2009
2010
2011
2012
2013
2014
2015
2016
2017
2018
2019
Date
Reference
This study
Fiorella et al. 2015
Guy et al. 2019
Elevation (m)
5000
4000
3000
2000
1000